A&A 422, 289–306 (2004)
DOI: 10.1051/0004-6361:20035860

Astronomy & Astrophysics

Dynamic model atmospheres of AGB stars

IV. A comparison of synthetic carbon star spectra with observations

R. Gautschy-Loidl[1], S. Höfner[2,5], U. G. Jørgensen[3], and J. Hron[4]

[1] Froburgstrasse 43, 4052 Basel, Switzerland
[2] Dept. of Astronomy and Space Physics, Uppsala University, Box 515, 75120 Uppsala, Sweden
[3] Niels Bohr Institute, Astronomical Observatory, Juliane Maries Vej 30, 2100 Copenhagen, Denmark
[4] Institut für Astronomie der Universität Wien, Türkenschanzstraße 17, 1180 Wien, Austria
[5] NORDITA, Blegdamsvej 17, 2100 Copenhagen, Denmark

Received 13 December 2003 / Accepted 8 April 2004

Abstract. We have calculated synthetic opacity sampling spectra for carbon-rich Asymptotic Giant Branch (AGB) stars based on dynamic model atmospheres which couple time-dependent dynamics and frequency-dependent radiative transfer, as presented in the third paper of this series. We include the molecules CO, CH, CN, C_2, CS, HCN, C_2H_2 and C_3 in our calculations, both when computing the atmospheric structures, and the synthetic spectra. A comparison of the synthetic spectra with various observed colours and spectra in the wavelength range between 0.5 and 25 μm of TX Psc, WZ Cas, V460 Cyg, T Lyr and S Cep is presented. We obtain good agreement between observations gathered at different phases and synthetic spectra of *one single* hydrodynamical model for each star in the wavelength region between 0.5 and 5 μm. At longer wavelengths our models showing mass loss offer a first self-consistent qualitative explanation of why a strong feature around 14 μm, which is predicted by all hydrostatic models as well as dynamical models showing no mass loss, is missing in observed AGB carbon star spectra.

Key words. stars: AGB and post-AGB – stars: atmospheres – stars: variables: general – stars: carbon – hydrodynamics – radiative transfer

1. Introduction

Large amplitude pulsations with periods of about 100 to 1000 days are characteristic for stars on the Asymptotic Giant Branch (AGB). Stellar pulsation creates strong shock waves in their atmospheres, causing a levitation of the outer layers. The density-temperature structure is highly dependent on dynamical phenomena, such as shock waves and stellar winds. In addition, the formation of molecules and dust grains plays a very important role for the atmospheric structures and the observable properties of these stars.

In the past, observed spectra of cool stars have been mostly analysed with synthetic spectra calculated from hydrostatic model atmospheres (e.g., Jørgensen 1989; Lambert et al. 1986; Goebel et al. 1980; Jørgensen et al. 2000; Ohnaka et al. 2000; Loidl et al. 2001, for carbon-rich stars; Tsuji et al. 1997b for oxygen-rich stars) or with simple blackbodies (e.g., Goebel et al. 1980). Spectra based on hydrostatic models are applicable for the description of giants showing no significant pulsation. But for an investigation of the effects of various time-dependent phenomena (shocks, stellar winds) on observable properties of pulsating AGB stars the use of dynamic models is the only self-consistent method.

Due to new instrumental developments during the last few years more and better observational data on AGB stars became available. The ISO mission provided for the first time full spectral coverage of the wavelength range between 2.5 and 197.6 μm and multi-epoch spectroscopic observations of carbon-rich AGB variables. This has made the shortcomings of hydrostatic standard model atmospheres more apparent, especially with regard to temporal variations in observed spectra and in photometric colours which are connected to stellar pulsation.

In the last few years, considerable progress has been made with regard to modelling of AGB star atmospheres. Bessell et al. (1989, 1996) have computed pioneering synthetic spectra for oxygen rich AGB stars based on dynamic model atmospheres, and Beach et al. (1988) analysed effects of pulsation on apparent diameters and broad band fluxes. For carbon-rich objects, Fleischer et al. (1992) and Höfner & Dorfi (1997) have presented the first sets of dynamic models which include time-dependent dust formation in a self-consistent way. For these models of circumstellar envelopes qualitative agreement with observable quantities like IR light curves (Winters et al. 1997)

Send offprint requests to: R. Gautschy-Loidl,
e-mail: rita@gautschy.ch

or IRAS colours (Windsteig et al. 1997) could be obtained. Hron et al. (1998) presented a first comparison of dynamical model spectra with ISO observations of R Scl. Recently, Tej et al. (2003) analysed the effects of the water molecule on diameter measurements in oxygen-rich stars using the dynamical models of Bessel et al. (1996) and Hofmann et al. (1998).

So far, dynamical modelling of C-stars has mainly concentrated on objects with high mass loss rates ($\dot{M} > 10^{-6}\,M_\odot\,\mathrm{yr}^{-1}$) and more or less optically thick dust envelopes, investigating the properties of the circumstellar dust shells and mass loss by dust-driven stellar winds (e.g., Höfner & Dorfi 1997; Winters et al. 2000). In Paper I (Höfner et al. 1998) and Paper III (Höfner et al. 2003) of this series we focused on the structure of the inner dust-free atmospheric regions. In AGB stars which are not completely obscured by an optically thick dust envelope, the visual and near infrared absorption spectra are mainly formed in this zone. Our recently developed model atmospheres couple time-dependent dynamics and frequency-dependent radiative transfer. This improvement was necessary in order to obtain reasonable atmospheric structures and realistic molecular features. Furthermore, we have improved these models by including a non-grey description of the dust component (see Höfner et al. 2003, for details). The new generation of dynamical models has been developed with the goal of predicting spectra of stars with low mass loss rates ($\dot{M} \leq 10^{-7}\,M_\odot\,\mathrm{yr}^{-1}$) and circumstellar envelopes of moderate optical depths which simultaneously show spectral features originating in photospheric layers and the stellar wind.

In this paper we present a comparison of our dynamic opacity sampling spectra with observations of TX Psc, WZ Cas, V460 Cyg, T Lyr and S Cep which cover the wavelength region from 0.5 to 25 μm. Several authors have analysed these stars by use of hydrostatic atmospheric models and assigned fundamental parameters and C/O ratios to them (e.g., Lambert et al. 1986; Aoki et al. 1998; Jørgensen et al. 2000). For example, TX Psc has been listed in the literature as having $T_{\rm eff}$ between 2800 K and 3200 K, and its carbon to oxygen abundance ratio has been estimated to values between 1.02 and 1.1. Obviously, the chemical abundance cannot be a function of phase for a given star, but it is also problematic to define the effective temperature of a cool variable star. The only really meaningful way of describing the observations of these stars, is to ascribe one pulsating model atmosphere to the star, and explain the different observations as different phases of this model. We attempt in this paper to identify such models, based on various photometric and spectroscopic observational material. This approach in principle gives information about the mass and the chemical abundances of the star, and it assigns fundamental parameters (T_*, L_*, R_*) to the hydrostatic initial model (which can be compared to $T_{\rm eff}$, L and $\log(g)$ in the traditional model atmosphere analysis and stellar evolution models).

2. Hydrodynamic models and spectral synthesis

2.1. Dynamic models

We use the dynamic model atmospheres developed by Höfner et al. (2003, Paper III in this series) for the calculation of synthetic spectra. To obtain the atmospheric structure, the coupled system of frequency-dependent radiation hydrodynamics and time-dependent dust formation is solved, employing an implicit numerical method and an adaptive grid. The dust formation is treated by the so-called moment method (Gail & Sedlmayr 1988; Gauger et al. 1990). A set of four equations which describe the time-dependent formation, growth and evaporation of grains is solved simultaneously with the radiation-hydrodynamics equations, providing information about the number density and average size of the grains, and the fraction of condensible material actually condensed into dust particles (degree of condensation). These quantities are sufficient to derive e.g. the dust opacity (provided the dust grains are small compared to the relevant wavelengths which is a fair approximation in this context) and to describe the effects of the newly formed grains on the dynamical atmosphere.

In contrast to earlier dynamic models, the treatment of the radiation field in the present dynamical simulations is frequency-dependent, including both gas and dust opacities (Höfner 1999; Höfner et al. 2003). The gas is represented by opacity sampling data of molecular opacities (SCAN data base, Jørgensen 1997) at 51 frequency points between 0.3 and 25 μm. The optical properties of the dust grains are calculated using the data for amorphous carbon by Roleau & Martin (1991). More details about the modelling method can be found in Höfner et al. (2003) and references therein.

The dynamical calculations start from hydrostatic initial models which are characterised by the following parameters: luminosity $L_\star$, mass $M_\star$, temperature $T_\star$ and the elemental abundances (all abundances except that of carbon are assumed to be solar). An initial model corresponds to the hydrostatic limit case of the radiation-hydrodynamical equations, assuming that no dust is present. It can be directly compared to classic model atmospheres.

The stellar pulsation of the AGB star is simulated by a variable inner boundary (piston) located beneath the stellar photosphere. The piston varies sinusoidally with a velocity amplitude $\Delta u_{\rm p}$ and a period P. The luminosity at the inner boundary varies proportional to the square of the radius of the inner boundary times a free parameter f_L, where $f_L = 1$ corresponds to our previously used boundary condition where the flux is kept constant at the radius of the inner boundary. The introduction of f_L allows us to adjust the amplitude of the luminosity variation to the observed values of the bolometric amplitude while keeping a given mechanical energy input (through $\Delta u_{\rm p}$). For fixed stellar parameters, the atmospheric structure is mostly determined by $\Delta u_{\rm p}$, and the influence of f_L is rather limited in that respect, at least for the range of values used in this paper. Note that most models discussed in this paper use the original boundary condition, i.e. $f_L = 1$.

The outer boundary of the hydrostatic initial models is relatively close to the photosphere, due to the strong density gradient in the atmosphere. During the dynamical calculation we allow the outer boundary to vary with the upper layers of the atmosphere in the case of dust-free models without wind. If a model develops a wind, the outflowing gas is traced out to about 20−30 $R_\star$ and there the outer boundary is fixed, allowing outflow of material. Experience shows that the wind in a fully

Table 1. Model parameters ($L_\star$, $M_\star$, $T_\star$, C/O; P, Δu_p, f_L; see Sect. 2.1) and results: mass loss rate $\dot{M}$, mean velocity at the outer boundary $\langle u \rangle$, mean degree of condensation at the outer boundary $\langle f_\mathrm{c} \rangle$; for convenience, we also list the corresponding $\lg g_\star$ and the full amplitude Δm_bol. Models which are discussed in the text in detail are marked with bold fonts.

Model	$L_\star$ [$L_\odot$]	$M_\star$ [$M_\odot$]	$T_\star$ [K]	$\lg g_\star$	C/O	P [d]	Δu_p [km s^{-1}]	f_L	Δm_bol [mag]	$\dot{M}$ [$M_\odot$ yr^{-1}]	$\langle u \rangle$ [km s^{-1}]	$\langle f_\mathrm{c} \rangle$
l52t34c11u2p	5200	1.0	3400	−0.19	1.10	148	2.0	1.0	0.13	–	–	–
l52t34c12u2p	5200	1.0	3400	−0.19	1.20	148	2.0	1.0	0.13	–	–	–
l52t32c11u2p	5200	1.0	3200	−0.30	1.10	148	2.0	1.0	0.10	–	–	–
l52t32c11u2	5200	1.0	3200	−0.30	1.10	295	2.0	1.0	0.13	–	–	–
l52t32c11u4	5200	1.0	3200	−0.30	1.10	295	4.0	1.0	0.44	–	–	–
l52t32c12u2p	5200	1.0	3200	−0.30	1.20	148	2.0	1.0	0.10	–	–	–
l52t32c12u2	5200	1.0	3200	−0.30	1.20	295	2.0	1.0	0.24	–	–	–
l52t31c14u2pim15	5200	1.5	3100	−0.18	1.40	180	2.0	1.0	0.13	–	–	–
l52t31c14u4pim15	5200	1.5	3100	−0.18	1.40	180	4.0	1.0	0.24	–	–	–
l52t31c14u2pim20	5200	2.0	3100	−0.06	1.40	180	2.0	1.0	0.13	–	–	–
l52t31c14u4pim20	5200	2.0	3100	−0.06	1.40	180	4.0	1.0	0.24	–	–	–
l52t30c05u4p	5200	1.0	3000	−0.41	1.05	148	4.0	1.0	0.15	–	–	–
l52t30c05u6pi	5200	1.0	3000	−0.41	1.05	186	6.0	1.0	0.31	–	–	–
l52t30c11u2	5200	1.0	3000	−0.41	1.10	295	2.0	1.0	0.20	–	–	–
l52t30c11u2f20	5200	1.0	3000	−0.41	1.10	295	2.0	2.0	0.41	–	–	–
l52t30c11u4	5200	1.0	3000	−0.41	1.10	295	4.0	1.0	0.41	–	–	–
l70t30c11u2	7000	1.0	3000	−0.54	1.10	390	2.0	1.0	0.23	–	–	–
l70t30c11u2f20	7000	1.0	3000	−0.54	1.10	390	2.0	2.0	0.46	–	–	–
l70t30c11u4	7000	1.0	3000	−0.54	1.10	390	4.0	1.0	0.46	–	–	–
l70t30c14u2	7000	1.0	3000	−0.54	1.40	390	2.0	1.0	0.24	–	–	–
l70t30c14u2f20	7000	1.0	3000	−0.54	1.40	390	2.0	2.0	0.48	–	–	–
l70t30c14u4	7000	1.0	3000	−0.54	1.40	390	4.0	1.0	0.48	–	–	–
l52t30c16u2	5200	1.0	3000	−0.41	1.60	295	2.0	1.0	0.21	–	–	–
l70t30c16u2	7000	1.0	3000	−0.54	1.60	390	2.0	1.0	0.24	–	–	–
l52t30c20u2pm20	5200	2.0	3000	−0.12	2.00	148	2.0	1.0	0.10	–	–	–
l70t28c11u2	7000	1.0	2800	−0.66	1.10	390	2.0	1.0	0.21	–	–	–
l70t28c11u4	7000	1.0	2800	−0.66	1.10	390	4.0	1.0	0.42	–	–	–
l70t28c14u2	7000	1.0	2800	−0.66	1.40	390	2.0	1.0	0.21	–	–	–
l70t28c14u4	7000	1.0	2800	−0.66	1.40	390	4.0	1.0	0.42	2.4×10^{-6}	11	0.28
l70t28c14u5	7000	1.0	2800	−0.66	1.40	390	5.0	1.0	0.53	3.5×10^{-6}	15	0.33
l10t28c14u2	10 000	1.0	2800	−0.82	1.40	525	2.0	1.0	0.20	–	–	–
l10t28c14u4	10 000	1.0	2800	−0.82	1.40	525	4.0	1.0	0.41	2.5×10^{-7}	14	0.22
l70t28c16u2	7000	1.0	2800	−0.66	1.60	390	2.0	1.0	0.21	–	–	–
l70t28c16u4	7000	1.0	2800	−0.66	1.60	390	4.0	1.0	0.42	6.6×10^{-7}	17	0.22
l70t28c20u2m20	7000	2.0	2800	−0.36	2.00	390	2.0	1.0	0.20	–	–	–
l70t28c20u4m20	7000	2.0	2800	−0.36	2.00	390	4.0	1.0	0.40	–	–	–
l10t26c14u2	10 000	1.0	2600	−0.94	1.40	525	2.0	1.0	0.20	3.6×10^{-6}	18	0.30
l10t26c14u4	10 000	1.0	2600	−0.94	1.40	525	4.0	1.0	0.41	5.9×10^{-6}	18	0.37
l10t26c14u4f20pi	10000	1.0	2600	−0.94	1.40	490	4.0	2.0	0.81	4.3×10^{-6}	15	0.28
l10t26c16u2	10 000	1.0	2600	−0.94	1.60	525	2.0	1.0	0.20	4.9×10^{-6}	26	0.39
l10t26c16u4	10 000	1.0	2600	−0.94	1.60	525	4.0	1.0	0.41	7.8×10^{-6}	24	0.40

developed model has usually reached its final outflow velocity at this distance.

2.2. Model parameters and wind properties

The parameters and properties of the models used for the calculation of the synthetic spectra are summarized in Table 1. If a stellar wind developed, the mass loss rate $\dot{M}$ is listed together with the asymptotic wind velocity u and the degree of condensation f_c. Note that all dynamical models were calculated allowing for the formation of dust grains and stellar winds, but many of the models discussed in this paper (in particular those with high effective temperatures, low C/O values and/or low pulsation amplitudes) result in dust-free pulsating atmospheres without mass loss.

In fact, the stellar parameters of the models in this paper were specifically chosen to produce atmospheres which are not significantly obscured by dusty circumstellar envelopes.

Table 2. Basic properties of our sample stars.

Star name	Var. type	Sp. type	P [days]	$\dot{M}$ [$M_\odot\,\mathrm{yr}^{-1}$]
TX Psc	Lb	C7,2	–	9.1×10^{-8} (1)
WZ Cas	SRb	C9,2	186	6.5×10^{-9} (2)
V460 Cyg	SRb	C6,4	180	1.8×10^{-7} (2)
T Lyr	Lb	C6,5	–	7.0×10^{-8} (2)
S Cep	M	C7,3	486.84	1.5×10^{-6} (2)

(1) From Olofsson et al. (1993).
(2) From Schöier & Olofsson (2001).

The latter would complicate the comparison with observations severely, due to the effects of uncertain micro-physical data for dust grains (see, e.g., Andersen et al. 2003), and possible ambiguities in observational constraints like the spectral energy distribution (see Sect. 5 for details). It should be noted here that only one star discussed here, S Cep, shows a significant mass loss rate in the sense that the spectrum at short wavelengths is altered noticeably. All other stars have mass loss rates of at least one order of magnitude lower (see Table 2), and they may be compared with "purely photospheric" models (i.e. such with no wind).

From the theoretical point of view, the production of wind models with very low mass loss rates is difficult. As demonstrated by several systematic studies (e.g., Höfner & Dorfi 1997; Winters et al. 2000) the transition from models without winds to models with considerable mass loss rates occurs in a very narrow range of stellar parameters (in particular $T_\star$, C/O and piston amplitude). Dust formation in AGB stars is usually proceeding far from equilibrium since the corresponding time scales are comparable to the ones which characterize the changes in the thermodynamical conditions in the stellar atmospheres (pulsation, shocks, etc.; see, e.g., Gustafsson & Höfner 2004, for simple estimates). This leads to a strongly non-linear response of dust formation to the thermodynamical conditions, and, via complex feedback mechanisms, to the sensitive dependence of the wind properties on the stellar parameters as mentioned above. In practice, this means that a very dense model grid is necessary to capture the transitions from windless models to noticeable outflows, covering a wide range of mass loss rates. Such a grid is beyond the scope of this paper, and therefore we have decided to use models without winds for the stars with low mass loss rates, instead of trying to produce such outflows which would not affect the resulting spectra in the most relevant spectral range.

2.3. Spectral synthesis

The dynamical calculation yields the structure of the atmosphere and circumstellar envelope (density, temperature, degree of condensation, etc.) as a function of time. Based on this structure we computed the synthetic spectra by evaluating (1) the chemical abundances of molecules using an equilibrium chemistry, (2) the continuum absorption using routines from the MARCS code (Gustafsson et al. (1975) in the version of Jørgensen et al. 1992) and (3) the molecular opacities as a function of wavelength using the opacity sampling method (as well as the dust opacities if the model formed dust). For the computation of the synthetic spectra we use a larger frequency set of our opacity samplings than the one used for the model construction. The spectral sampling density corresponds to a resolution of approximately 20 000 in the wavelength range between 0.3 and 25 μm. We include the molecules CO (from Goorvitch & Chackerian 1994), CN (from Jørgensen & Larsson 1990), C_2 (from Querci et al. 1974), CH (from Jørgensen et al. 1996), CS (from Chandra et al. 1995), HCN, C_2H_2, and C_3 (as described in Jørgensen 1997) in the opacity, together with continuum sources as described in Gustafsson et al. (1975). The CN opacities have been improved compared to Jørgensen & Larsson (1990), by including also the violet system, and the C_2 opacities have been modified somewhat in the infrared spectral range as described in Loidl et al. (2001). The molecular dissociation energies are from Tsuji (1973), Sauval & Tatum (1984) and Irwin (1981, 1988), with minor updates. For this work the values of particular importance are those for CN from Costes et al. (1990) and for C_3 which is scaled as described in Jørgensen et al. (2000). Compared to our previous systematic investigation of synthetic spectra of dynamical model atmospheres (Loidl et al. 1999) and a first comparison of these spectra with ISO observations of R Scl (Hron et al. 1998), the model structures here are improved by being based on non-gray radiative transfer (Höfner et al. 2003), and the synthetic spectra are now calculated with a spherically symmetric radiative transfer (instead of plane parallel), and frequency-dependent dust opacities for amorphous carbon are included in our spectra using the data of Roleau & Martin (1991).

3. Observations

We use spectra which were obtained with four different telescopes during the last 30 years: The first data set are spectra which were observed with the **K**uiper **A**irborne **O**bservatory (KAO) in the years 1976 to 1978 (Goebel et al. 1978). These spectra cover the wavelength region between 1.23 and 5.5 μm simultaneously. The spectral calibration is based on observations of Vega and on the assumption that its energy distribution may be described by a 10 000 K blackbody in the wavelength region between 1.2 and 4 μm. Strecker et al. (1978) report that for sources which were observed during two successive nights with the KAO a comparison of spectral shape and absolute signal level showed agreement of ±2%. We assume the accuracy of the calibrated spectra to be 5% or better.

The second data set are spectra which were observed by Lázaro et al. (1994) during two campaigns in 1983 and 1985. Both times the Carlos Sanchez Telescope (TCS) of the Observatorio del Teide in Tenerife was used. The observations were made by driving the grating at a constant speed across the various wavelengths of interest (1.0−1.40 μm, 1.50−1.90 μm, 1.90−2.45 μm and/or 2.9−4.20 μm). The spectra have a resolution of about 500. Vega was used for the flux calibration and in order to determine the air mass extinction. The difference in air

masses within a scan can be appreciable. This is important at wavelengths with strong water telluric lines. For the conversion to absolute fluxes an ATLAS6 model atmosphere of Vega was used. Lázaro et al. (1994) estimate the accuracy of their calibrated spectrophotometry to be 6% between 1.0 and 1.08 μm and 5% between 1.4 and 4.1 μm. We assume the accuracy of the gradients within a band to be better than 5% and the accuracy of the absolute fluxes and the overall gradients to be about 10%.

The third data set contains spectra obtained by Joyce (1998) with the 1.3 m telescope at Kitt Peak National Observatory using the IR cryogenic spectrograph CRSP in 1991. These spectra have a resolution of about 250 and they cover the wavelength range between 1.08 and 1.83 μm, between 1.99 and 2.53 μm, and between 2.88 and 4.16 μm. Due to nonphotometric conditions the spectra were not flux-calibrated. The spectra were "pseudocalibrated" by converting the telluric-corrected spectra to a logarithmic magnitude scale and setting the average value over the standard photometric filter bandpass to a published value for the object. They were then converted to fluxes by using a blackbody with 11 400 K which is an empirically determined best fit to observed infrared spectra of Vega. Tying the flux calibration of spectra to photometry obtained several years previous assumes the star to be nonvariable, which is a dangerous assumption in the case of carbon-rich AGB stars. Thus we assume the accuracy of the gradients within a band to be better than 5% and the accuracy of the absolute fluxes and the overall gradients to be about 10% based on the fact that our objects are Lb and SRb variables, for Miras the accuracy may be significantly worse than 10%.

The forth and last data set contains spectra obtained with the Short-Wavelength-Spectrometer (SWS; de Graauw et al. 1996) on board of the **I**nfrared **S**pace **O**bservatory (ISO) which was operated between November 1995 and April 1998. Its grating spectrometers cover the wavelength region 2.36–45.2 μm, with an overall spectral resolution of about 200 for the SWS01 and a resolution of about 1000 for the SWS06. The speed of the used SWS01 observations was either 1 or 2. All our pipeline processed ISO data (OLP versions 8.7 and 9.5) were further reduced with the ISO Spectroscopic Analysis Package (`http://www.ipac.caltech.edu/iso/isap/isap.html`). First, we removed bad data points, then the 12 bands were cut shortwards and longwards of those wavelengths where the data are not reliable anymore. As a next step we checked whether one or more of the 12 detectors produced abnormal spectra, which happened quite often. We checked whether a significant offset existed between the data points recorded in the two scan directions, if so, the down-scan direction was rejected in the SWS01 data. In the case of the SWS06 data the average of the two scan directions has been used. For the joining of the bands we used band 1A (2.36–2.61 μm) as a flux reference. Between all 12 bands short regions of overlap exist. We calculated the mean flux values of the neighbouring bands in the overlap region. The averaging of the detectors and the way of joining the 12 bands is crucial for the final appearance of the ISO spectra and hence for the interpretation of the data. Following the instructions of the ISO calibration team, the individual detectors in a band were corrected to a mean value by additive constants if the flux was below 200 Jy and by multiplicative corrections otherwise. For the joining of the bands, originally the same procedure was suggested by the ISO calibration team. However, this change of the way of correction at a certain flux level influences the overall shape of the spectrum dramatically for most of our sample stars as they have low fluxes. We tested different reduction methods by comparing five K giants and three moderately variable AGB stars surrounded by almost no dust with the IRAS fluxes and continua of model spectra. Based on these results we concluded in accordance with members of the ISO calibration team (Kieron Leech, private communication) that for joining the bands we should use multiplicative corrections all over the spectrum, no matter what the actual flux level is. As a final step we smoothed the spectra and rebinned them to the desired resolution. The standard deviation is up to 1% to 10 μm for our ISO data. Thus we assume the accuracy within a band to be <5% (typically 1% in regions with high fluxes) and the accuracy of the absolute fluxes and the overall gradients to be about 5%.

Colour measurements in the optical and the NIR wavelength range were taken from Baumert (1972). The Photometric System used in Baumert's study is a system of eight interference filters specifically designed for the study of late-type stars with the central wavelengths at 0.7117, 0.7544, 0.7809, 0.8122, 1.0395, 1.0544, 1.0804, and 1.0975 μm. This system is described in Wing (1971). These observations were obtained at three different observatories with seven telescopes and three photometers (Baumert 1972). Baumert lists his colour measurements normalised to the flux of Vega at 1.0395 μm for *all* filters. The Vega flux at 1.0395 μm is assumed to have zero magnitude. Thus the observed colour measurements were converted to fluxes by using the relation $\mathrm{mag}_x = -2.5 \times \log(F_x/F_{1.0395})$.

4. Comparison of synthetic spectra of dust-free windless models with observations

In this section we will compare observed colours and spectra in the wavelength region between 0.5 and 25 μm of TX Psc, WZ Cas, V460 Cyg, and T Lyr with our dynamical model spectra. Table 2 lists the basic properties of all our sample stars.

4.1. Fit criteria and model grid

For each of the stars investigated here we intend to describe all observations between 0.5 and 25 μm reasonably well with one dynamical model from our grid. As main diagnostic tools for the estimation of the temperature of the star we use the 2.5, 3 and 3.8 μm C_2H_2 /HCN feature intensities as well as the overall shape of the energy distribution (for stars with low mass loss rates) which should be described correctly. For the estimation of the C/O ratio the intensity of the 5.1 μm C_3 feature is used. We use these features because Gautschy-Loidl (2001) showed that their feature intensities are reacting very sensitively to changes in temperature and C/O ratio respectively. The CN and C_2 feature intensities in the wavelength region between 0.5 and about 2 μm are only used as secondary tool for parameter estimations due to some uncertainties in the opacity

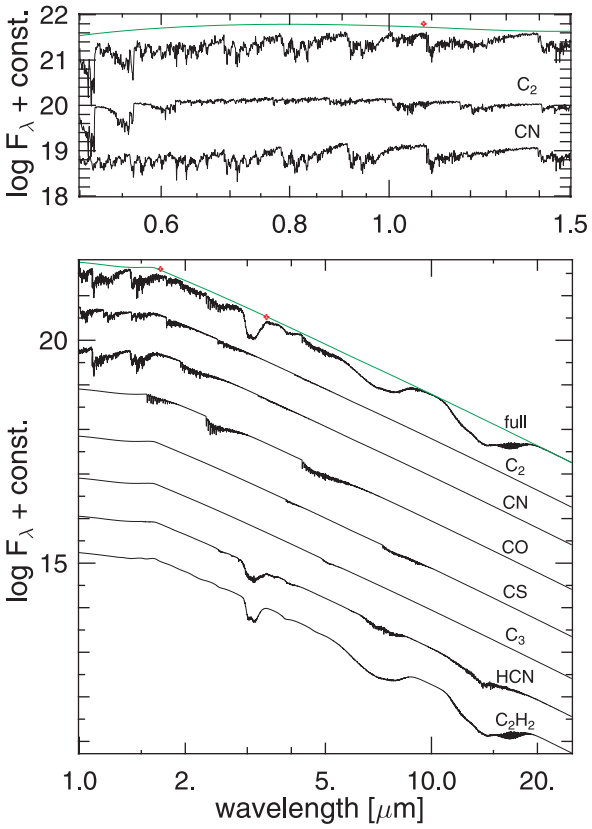

Fig. 1. *Upper panel*: full synthetic spectrum at minimum phase of model l52t32c11u4 in the wavelength region between 0.5 and 1.5 μm (top black line), the continuum (grey line) and the contributions of C_2, and CN. *Lower panel*: full synthetic spectrum in the wavelength region between 1 and 25 μm (black line), the continuum (grey line) and the contributions of C_2, CN, CO, CS, C_3, HCN, and C_2H_2. Crosses denote wavelengths which were used to normalise observations and model spectra.

data of C_2 which are discussed in detail in Loidl et al. (2001). Figure 1 shows the contributions of single molecules to the full spectrum for phase 0.50 of model l52t32c11u4. The grey line shows the continuum, the crosses denote wavelengths which were used to normalise observations and model spectra.

The piston velocity Δu_p is responsible for the amount of variation of the spectral features during a pulsation period. All other model parameters ($L_\star$, $M_\star$, P) have only a minor influence on the appearance of the resulting spectra compared to the temperature and the C/O ratio. All our models and synthetic spectra are calculated with opacity data computed for a microturbulent velocity of 3 km s^{-1} and a ^{12}C/^{13}C ratio of 89 (which is the solar value). From our detailed comparison of plane parallel hydrostatic model spectra with observations (Loidl et al. 2001) we know that varying the ^{12}C/^{13}C ratio between 3.5 (the CNO cycle equilibrium, which is the theoretical minimum value) and 89 typically results in a best fit obtained with a difference in effective temperature of 100 K and a difference in the C/O ratio of about 0.05. But it would be far beyond the scope of this paper to vary also these parameters in our current dynamical models.

To find a model matching the observed spectra for each star we proceeded in two steps. First, we extended the model grid presented in Höfner et al. (2003) using a predefined sequence of luminosities (5200, 7000 and 10 000 $L_\odot$) and effective temperatures (3400, 3200, 3000, 2800 and 2600 K) in combination with different values of C/O (1.1 and 1.4) and keeping the stellar mass constant. As in the previous paper, the pulsation periods (295d, 390d and 525d) are related to the luminosities through an observed $P - L$ relation and the piston velocity amplitudes are chosen as $\Delta u_\mathrm{p} = 2$ or 4 km s^{-1} [1]. After selecting the closest matching model from this first grid we further adjusted one or more parameters of the model (notably C/O, P, Δu_p, $M_\star$) if it was necessary to get a better fit.

The dynamical model which resulted in spectra matching closest all our observations in the wavelength range between 0.5 and 25 μm of a specific star we denote as "best fit model" for this star. It should be stated, however, that we cannot exclude the possibility that a fit of equal quality may be obtained with another set of parameters (see also Jørgensen et al. 2000). Thus we discuss for each star how sensitively, and in which way, the synthetic spectra depend on the chosen stellar parameters. We also want to state that at this stage the fitting of synthetic to observed spectra should rather be regarded as a way of testing the dynamical models than as an independent way of determining stellar parameters.

For the comparison with the four only moderately variable stars (which show semiregular or irregular variations) we did not assign phases to the observed spectra and compare them with the corresponding model phases, but we simply chose the model phases describing the observed spectra best. Our dynamical atmospheres are not based on pulsational models, but a piston located beneath the stellar photosphere is responsible for the variations, and the changes of the bolometric luminosity at this location have to be specified explicitly (cf. Sect. 2.1). This may result in offsets between the "mechanical behaviour" (density-temperature structure, propagating waves) and the corresponding luminosity phase of the models relative to the observations. Preliminary results by Nowotny et al. (2004) show reasonable agreement of line profile variations (radial velocities) of the CN 0–2 red bands at 1.995 μm and second overtone lines of CO resulting from our models with observed variations as a function of phase. However, these lines form relatively deep in the atmospheres, mainly at temperatures above 3000 K. On the other hand, the molecular features which dominate the low-resolution spectra discussed here, and which are used as fit criteria in this paper, partly form in the upper layers of the atmospheres or the inner wind region (at temperatures below 2200 K). These layers may not even vary periodically with the piston period but can show a multi- or non-periodic behaviour. This leads to uncertainties in the association of the synthetic spectra with observed phases (see also Sect. 5).

[1] Note that not all combinations of these values were used for the primary grid, but a "band" of models with the luminosity and C/O increasing with decreasing effective temperature, as expected from evolution models. In addition, we also calculated models with a shorter period (half the value obtained from the $P - L$ relation) in some selected cases.

Table 3. Observations and stellar parameters.

Parameter	TX Psc			WZ Cas			V460 Cyg			T Lyr		
$T_{\rm eff}$, C/O, log g:												
Ohnaka (1997)	3080	1.16	0.0	3160	–	0.0	3230	–	0.0	–	–	–
Lambert et al. (1986)	3030	1.027	0.0	2850	1.010	0.0	2845	1.062	0.0	2380	1.29	0.0
Aoki et al. (1998)	3080	1.10	0.0	2900	1.01[(1)]	0.0	–	–	–	–	–	–
Jørgensen et al. (2000)	3100	1.10	0.0	–	–	–	3000	1.20	−0.5	–	–	–
This work	3200	1.10	−0.3	3000	1.05	−0.41	3400	1.20	−0.19	3000	2.00	−0.12
							3100	1.40	−0.18	2800	1.60	−0.66

[(1)] C/O ratio adopted from Lambert et al. (1986).

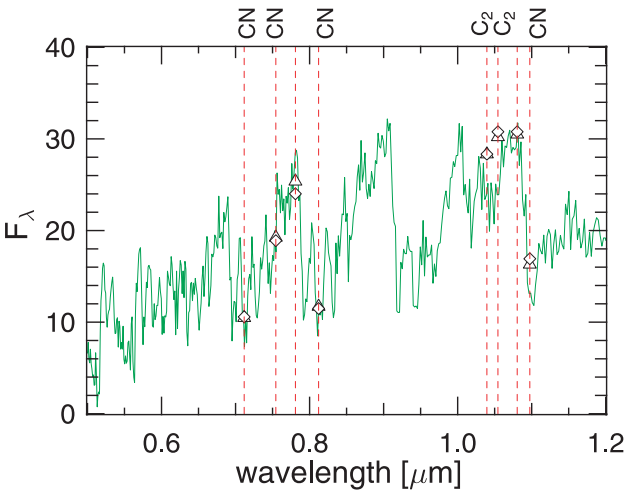

Fig. 2. Comparison of a l52t32c11u4 minimum (phase 0.50) model spectrum with the Baumert observations of TX Psc. The maximum values of his colour measurements are denoted by triangles, the minimum values by diamonds. On top of the figure the *main* contributing molecule is labelled.

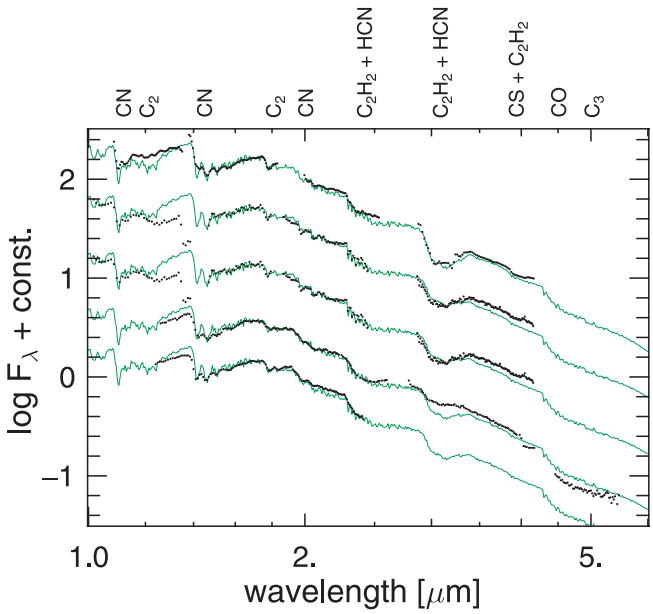

Fig. 3. Comparison of l52t32c11u4 model spectra (grey lines) with the following observational data (black lines) of TX Psc (from top to bottom): one spectrum from Joyce (1998); two spectra from Lázaro et al. (1994); and two KAO spectra. The model phases are (from top to bottom): 0.83, 0.66, 0.71, 0.71, and 0.66. On top of the figure the *main* contributing molecules are labelled.

4.2. TX Psc

TX Psc is the brightest carbon star and hence it is among the best studied ones. Numerous observational data exist. We selected data of Baumert (1972), of Lázaro et al. (1994), two spectra obtained by the KAO (Martin Cohen, private communication), a spectrum by Joyce (1998), and three ISO SWS spectra. TX Psc is an irregular variable (Lb) star and Olofsson et al. (1993) list a mass loss rate of $9.1 \times 10^{-8}\,M_\odot\,{\rm yr}^{-1}$.

We obtained the best fit of all our observational data with model l52t32c11u4 ($T_\star = 3200\,{\rm K}$, $L_\star = 5200\,L_\odot$, $M_\star = 1\,M_\odot$, C/O = 1.1 for the hydrostatic initial model; $P = 295\,{\rm d}$, $\Delta u_{\rm p} = 4\,{\rm km\,s}^{-1}$). These values are in good agreement with parameter determinations for TX Psc from other authors (see Table 3 and Jørgensen et al. 2000, for a more detailed summary for this star), as may be expected for a relatively warm star with a moderate amplitude of variability.

Figure 2 shows a comparison of phase 0.50 (minimum) of model l52t32c11u4 with the Baumert observations. Baumert (1972) measured TX Psc at ten epochs between November 1969 and June 1971. We adopted the maximum and minimum values of his colour measurements; the maximum values (i.e. the warmest colour temperature) are denoted by triangles in Fig. 2, the minimum values (i.e. the coolest colour temperature) by diamonds. Minimum observations and models were forced to have equal flux at 1.0804 μm because this seems to be the wavelength where we reach closest to the real continuum. We see that the overall shape of the energy distribution is very well represented by our model, only the contributions of C_2 at 1.0395 and 1.0544 μm are too strong.

In Fig. 3 the following observational data (black dotted lines) are plotted from top to bottom: a spectrum obtained by Joyce (1998) in September 1991; two spectra from Lázaro et al. (1994) obtained in 1983 and 1985; and two spectra by KAO observed in June 1976 and September 1976. Observed (black) and model spectra (grey lines) were forced to have equal flux at 1.7 μm because this wavelength is covered in all observations and additionally it is close to the centre of the H band. The model spectra were rebinned to a resolution of 250 for this comparison. We see that while the first

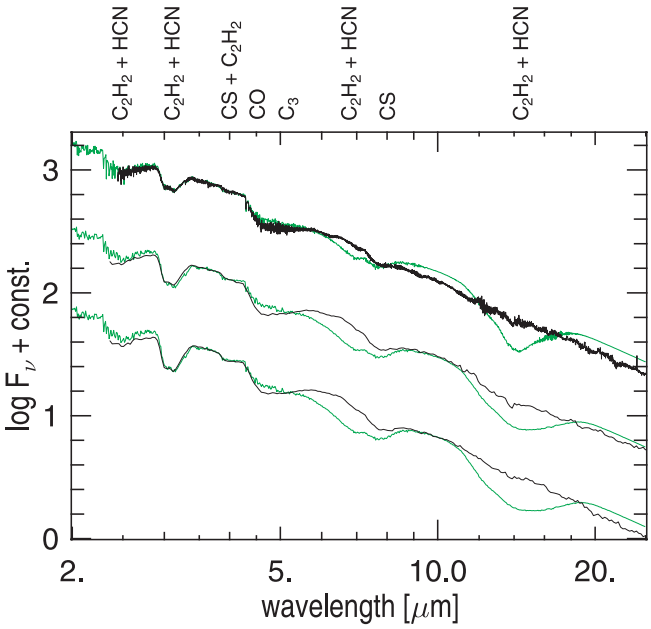

Fig. 4. Comparison of l52t32c11u4 model spectra (grey lines) with ISO SWS06 and ISO SWS01 spectra (black lines) of TX Psc. The model phases are (*from top to bottom*): 0.66, 0.71, and 0.83. On top of the figure the *main* contributing molecules are labelled.

three observed spectra (from the top) can be fitted well in the 1.4 to 5 μm range, our model is not able to describe the very weak 3 μm C_2H_2/HCN feature at any phase which was observed with KAO in June 1976 (second spectrum from the bottom). The intensities of the CN band at 1.46 and of the C_2 band at 1.77 μm are well reproduced by our synthetic spectra, thus giving an independent confirmation of our determination of the temperature (in the case of the CN band) and the C/O ratio (in the case of the C_2 band) which relies mainly on the intensities of the C_2H_2, HCN and C_3 features. The discrepancy between our synthetic spectra and especially the Lázaro observations in the wavelength region between 1.2 and 1.4 μm is probably due to the influence of the atmospheric water absorption at these wavelengths since the same wavelength region is described reasonably well in the comparison with the KAO spectra which are not influenced by the atmospheric water absorption. The overall slope of the observed spectra between 1 and 5 μm is represented well by our dust-free dynamical model. Thus we can conclude that we see a pure photospheric spectrum in this wavelength region. The very small discrepancies are consistent with flux calibration uncertainties of about 10% in the observed spectra.

In Fig. 4, one ISO SWS06 spectrum and two ISO SWS01 spectra are shown. The uppermost spectrum was observed in November 1996, the middle one in May 1997, and the lower one in December 1997. When looking at the 3 μm C_2H_2/HCN feature, one can see that the star cooled between the first and the last ISO observation. Observed (black lines) and model (grey lines) spectra were forced to have equal flux at 3.4 μm because this wavelength is close to the centre of the L band and thus very well covered in all observations and because it is at the edge of the 3 μm feature. The model spectra were rebinned to a resolution of 500 (for comparison with the SWS06 observation) or to a resolution of 250 (for comparison with the SWS01 observations).

We focused on fitting the 2.5, 3 and 3.8 μm C_2H_2/HCN features in this wavelength range. In the case of TX Psc we see basically a pure photospheric spectrum and our dynamical l52t32c11u4 model spectra should be able to describe this wavelength region correctly. At wavelengths longwards of 7 μm we have to expect to see the influence of the circumstellar envelope which we are not able to account for with our wind-free l52t32c11u4 model.

While we are able to describe the observed spectra between 2.4 and 4 μm well, we see a discrepancy between the observed and the dynamical model spectra in the wavelength region 5.5 to 7 μm. It barely exists in the hottest spectrum of the star. However, it becomes progressively more pronounced towards lower temperatures. Our model spectra do not reproduce correctly the shape of the long-wavelength side of the 5 μm feature, which is due to C_3 (the short wavelength side is due to the fundamental band of CO). The computed band that stretches from approximately 6 to 8.5 μm is dominated by C_2H_2/HCN shortward of 7 μm and by CS longward of 7 μm. It is remarkable that the observed spectrum is dominated by CS, while HCN and C_2H_2 are almost invisible in this region of the spectrum (as in the 14 μm region). Seemingly we see the deep photosphere (CS) in this region, while the HCN (and C_2H_2) absorption we expect in the higher layers are invisible. Our dynamical models predict too strong C_2H_2 absorption in the 6 to 7 μm region, like hydrostatic spherical models do (Gautschy-Loidl 2001). The fact that this problem does not show up in *plane parallel* model spectra (Jørgensen et al. 2000) hints at an additional absorption originating from the outermost model layers[2].

The discrepancy at wavelengths longer than 10 μm is most likely due to a non-photospheric contribution and will be discussed separately in Sect. 6.

We conclude that we can quite well explain observed spectra of TX Psc self-consistently with synthetic spectra of one dynamical model in the wavelength range between 0.5 and 5 μm.

4.2.1. Influence of model parameters on the fit

For TX Psc we obtained a best simultaneous fit of all observed spectra and colour measurements with model l52t32c11u4 ($T_\star = 3200$ K, $L_\star = 5200\,L_\odot$, $M_\star = 1\,M_\odot$, C/O = 1.1 for the hydrostatic initial model; $P = 295$ d, $\Delta u_\mathrm{p} = 4$ km s^{-1}).

The most important parameter is the temperature of the star. If the temperature is only about 100 K higher the 3 μm C_2H_2/HCN feature will be considerably weaker. But a model with higher effective temperature which would be able to explain also the very weak 3 μm C_2H_2/HCN feature observed with the KAO fails to describe the overall energy distribution correctly. Other parameters like the luminosity (e.g. $7000\,L_\odot$ instead of 5200) and mass (e.g. $1.5\,M_\odot$ instead of 1) have a

[2] The spherical model structures have lower temperatures at a fixed pressure than plane parallel ones and hence the partial pressures of C_2H_2 (and HCN) are considerably higher in the spherical case.

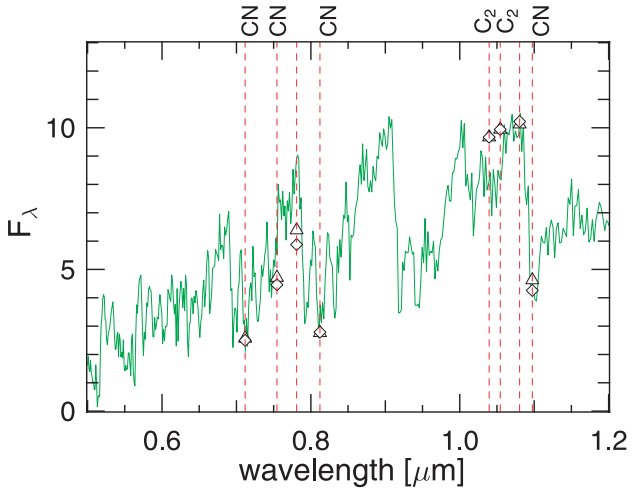

Fig. 5. Comparison of a l52t30c05u6pi minimum model spectrum (phase 0.52) with the Baumert observations of WZ Cas. The maximum values of his colour measurements are denoted by triangles, the minimum values by diamonds. On top of the figure the *main* contributing molecule is labelled.

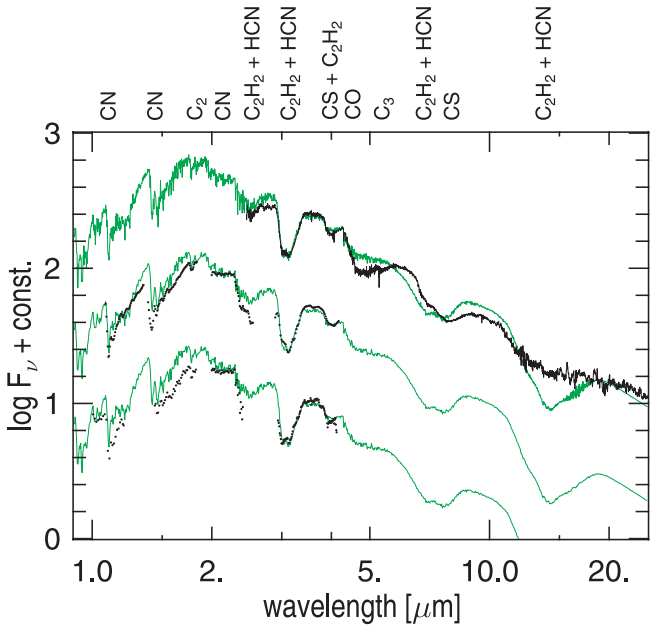

Fig. 6. Comparison of l52t30c05u6pi model spectra (grey lines) with the following observational data (black lines) of WZ Cas (from top to bottom): one ISO SWS06 spectrum; on spectrum from Joyce (1998); and one spectrum from Lázaro et al. (1994). The model phases are (from top to bottom): 0.83, 0.89, and 0.83. On top of the figure the *main* contributing molecules are labelled.

much smaller influence on the resulting feature intensities than a change in temperature. A higher C/O ratio results mainly in a stronger C_3 feature at 5.1 μm and in stronger C_2 features between 0.5 and 3 μm. A common feature is (see also Sects. 4.3–4.5) that our models predict too strong contributions of C_2 at 1.0395 and 1.0544 μm while at the same time we are able to explain the C_2 feature at 1.77 μm very well and while we are not able to explain the strong observed C_3 feature at 5.1 μm in stars with a C/O ratio significantly higher than 1. This is probably due to some uncertainties in the opacity data of C_2 which are discussed in Loidl et al. (2001). Changing the period to e.g. half of its value in dust-free and windless models has on first sight an astonishing effect: all features become considerably stronger. The reason for this is that the atmosphere has less time between successive shocks to relax, and as a consequence the levitation of the atmosphere is stronger. This results in higher partial pressures of polyatomic molecules like HCN or C_2H_2 which causes the stronger feature intensities of e.g. the 3 μm and the 3.8 μm features which we use as main diagnostic tools to determine the temperature. A higher piston velocity Δu_p causes stronger variations of the feature intensities.

4.3. WZ Cas

For the SRb variable WZ Cas, observational data of Baumert (1972), of Lázaro et al. (1994), of Joyce (1998), and one ISO SWS06 spectrum were available. Schöier & Olofsson (2001) list a mass loss rate of $6.5 \times 10^{-9}\,M_\odot\,\mathrm{yr}^{-1}$.

The best fit was obtained with model l52t30c05u6pi ($T_\star = 3000$ K, $L_\star = 5200\,L_\odot$, $M_\star = 1\,M_\odot$, C/O = 1.05 for the hydrostatic initial model; $P = 186$ d, $\Delta u_p = 6\,\mathrm{km\,s}^{-1}$). These values are in good agreement with parameter determinations for WZ Cas from other authors (see Table 3).

Figure 5 shows a comparison of a minimum model spectrum (phase 0.52) with the Baumert observations. Baumert (1972) measured WZ Cas four times between November 1969 and November 1970. We took the maximum and minimum colour values of his measurements, the maximum values are denoted by triangles in Fig. 5, the minimum values by diamonds. Minimum observations and models were forced to have equal flux at 1.0804 μm. The CN feature intensities at 0.7117 ($\Delta v = +3$), 0.8122 ($\Delta v = +2$) and at 1.0975 μm (0, 0) of our model spectrum are well represented, but the contributions of C_2 at 1.0395 and 1.0544 μm are too strong.

In Fig. 6, one ISO SWS06 spectrum obtained in July 1996 (top), and data from Joyce (1998) which were obtained in September 1991 (middle), and a spectrum by Lázaro et al. (1994) observed in 1983 (bottom) are shown. Observed (black lines) and model (grey lines) spectra were forced to have equal flux at 3.4 μm. The model spectra were rebinned to a resolution of 500 (for comparison with the SWS06 observation) or to a resolution of 250 (for comparison with the Joyce and Lázaro observations). We are able to describe the shape of the 3 and the 3.8 μm C_2H_2/HCN feature correctly and also the observed overall energy distribution is well represented. However, there remain discrepancies at wavelengths longwards of 4.5 μm. The CO feature at 4.6 μm in our model spectra is too weak, the contribution of C_2H_2 in the 6 to 7 μm region too strong, and also the synthetic CS feature around 8 μm may be too strong. WZ Cas is the star with the lowest mass loss rate in our sample, thus we can not expect that the influence of dust is responsible for the discrepancies in these wavelength regions. The discrepancy between models and the Joyce and Lázaro observations starting at about 2.3 to 2.4 μm are

possibly due to the influence of the atmospheric water absorption at these wavelengths.

The discrepancy at wavelengths longer than 10 μm will be discussed separately in Sect. 6.

We conclude that we can quite well explain observed spectra of WZ Cas self-consistently with synthetic spectra of one dynamical model in the wavelength range between 0.5 and 4.5 μm and that we see a pure photospheric spectrum at wavelengths shortwards of about 10 μm.

4.3.1. Influence of model parameters on the fit

For WZ Cas we obtained a best simultaneous fit of all observed spectra and colour measurements with model l52t30c05u6pi ($T_\star = 3000$ K, $L_\star = 5200\,L_\odot$, $M_\star = 1\,M_\odot$, C/O = 1.05 for the hydrostatic initial model; $P = 186$ d, $\Delta u_\mathrm{p} = 6$ km s^{-1}). The adopted C/O ratio of 1.05 may be slightly too high, Lambert et al. (1986) determined a C/O ratio of 1.01 which was later adopted also by Aoki et al. (1998). However, Lamberts C/O values are lower for all the stars investigated in this and our earlier papers (see e.g., Jørgensen et al. 2000), and it is far beyond the scope of the current dynamical models to determine the C/O ratio of a star with a higher precision than 0.05[3]. Therefore our grid of dynamical models currently does not include models with C/O ratios closer to 1 than 1.05. However, the fact that the CO band at 4.6 μm is too weak, the contributions of C_2 around 1.04 μm and the 7 μm C_2H_2 feature too strong in our model spectra hints at that our adopted C/O ratio for WZ Cas is indeed too high. As diagnostic tool for the determination of the temperature we used the intensity of the 3 and the 3.8 μm C_2H_2/HCN features and the overall shape of the energy distribution. A lower temperature makes it impossible to fit the 3 and 3.8 μm feature simultaneously, a higher temperature on the other hand decreases the quality of the fit of the overall energy distribution. All other model parameters (luminosity, mass, period, piston velocity) have the same influences as discussed in Sect. 4.2.1.

4.4. V460 Cyg

For the SRb variable V460 Cyg, observational data of Baumert (1972), of Lázaro et al. (1994), two ISO SWS01 spectra, and one ISO SWS06 spectrum (between 2.8 and 5.1 μm) were available. Schöier & Olofsson (2001) list a mass loss rate of $1.8 \times 10^{-7}\,M_\odot$ yr^{-1}.

We obtained the best fit with model l52t34c12u2p ($T_\star = 3400$ K, $L_\star = 5200\,L_\odot$, $M_\star = 1\,M_\odot$, C/O = 1.2 for the hydrostatic initial model; $P = 148$ d, $\Delta u_\mathrm{p} = 2$ km s^{-1}). These values are in fair agreement with parameter determinations for V460 Cyg from other authors (see Table 3). Figure 7 shows a comparison of our dynamical model spectra with the Baumert observations.

Baumert (1972) measured V460 Cyg four times between November 1969 and November 1970. We took the maximum and minimum colour values of his measurements, the maximum values are denoted by triangles in Fig. 7, the minimum values by diamonds. Minimum observations and models were forced to have equal flux at 1.0804 μm. We see that the overall shape of the energy distribution is well represented by our model. The C_2 features at 1.0395 and 1.0544 μm are too strong.

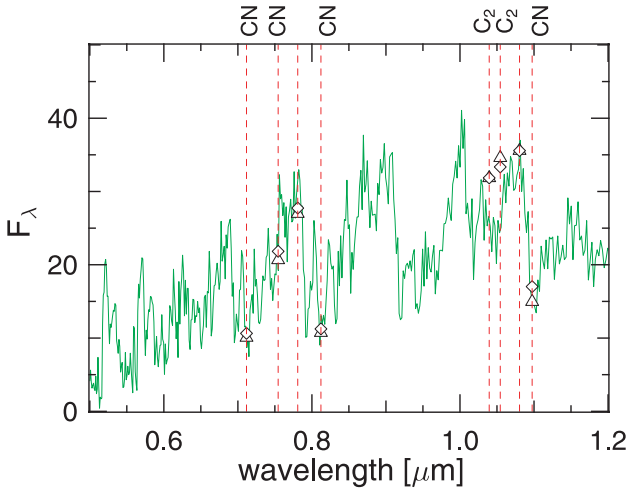

Fig. 7. Comparison of a l52t34c12u2p minimum (phase 0.51) model spectrum with the Baumert observations of V460 Cyg. The maximum values of his colour measurements are denoted by triangles, the minimum values by diamonds. On top of the figure the *main* contributing molecule is labelled.

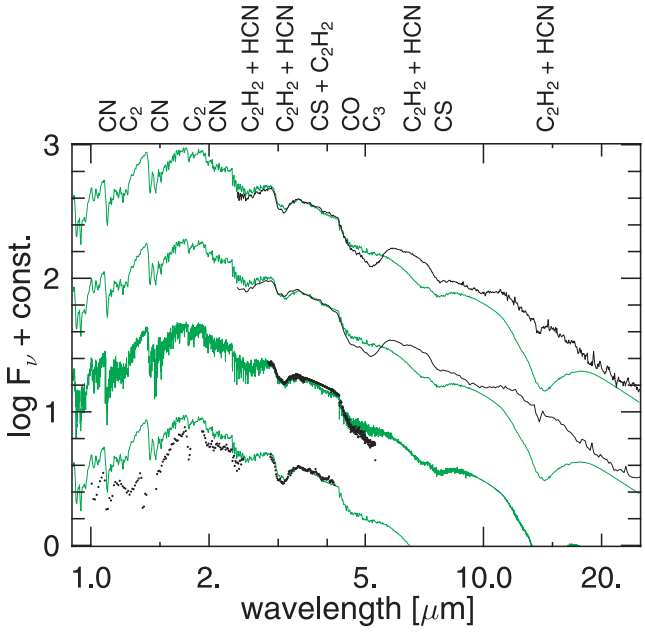

Fig. 8. Comparison of l52t34c12u2p model spectra (grey lines) with the following observational data (black lines) of V460 Cyg (from top to bottom): two ISO SWS01 spectra, one ISO SWS06 spectrum, and one spectrum from Lázaro et al. (1994). The model phases are (*from top to bottom*): 0.54, 0.56, 0.56, and 0.57. On top of the figure the *main* contributing molecules are labelled.

In Fig. 8, one ISO SWS01 spectrum from January 1997, one ISO SWS01 spectrum from November 1997, one ISO SWS06 spectrum, obtained in November 1997, and a spectrum by Lázaro et al. (1994) observed in 1983 are shown.

[3] Concerning this point see also the short discussion in Sect. 4.1 about the influence of the $^{12}C/^{13}C$ ratio on the "best fit".

Observed (black lines) and model (grey lines) spectra were forced to have equal flux at 3.4 μm. The model spectra were rebinned to a resolution of 500 (for comparison with the SWS06 observation) or to a resolution of 250 (for comparison with the ISO SWS01 and Lázaro observations). We are able to describe the region between 2.4 and 4.6 μm correctly. The discrepancy in the overall shape and thus the mismatch at wavelengths shortwards of about 2.5 μm and longwards of 6 μm is due to the fact that our best fit model is a dustless and wind-free model which is not able to reproduce the overall shape of the spectral energy distribution of a star which shows a considerable mass loss. The adopted C/O ratio of 1.2 is too low to describe the C_3 feature at 5.1 μm correctly. On the other hand the contribution of C_2H_2 in the 7 μm region is too strong. Around 11 μm V460 Cyg shows a weak SiC dust feature which is not included in our calculations. The discrepancy at wavelengths longer than 10 μm will be discussed separately in Sect. 6.

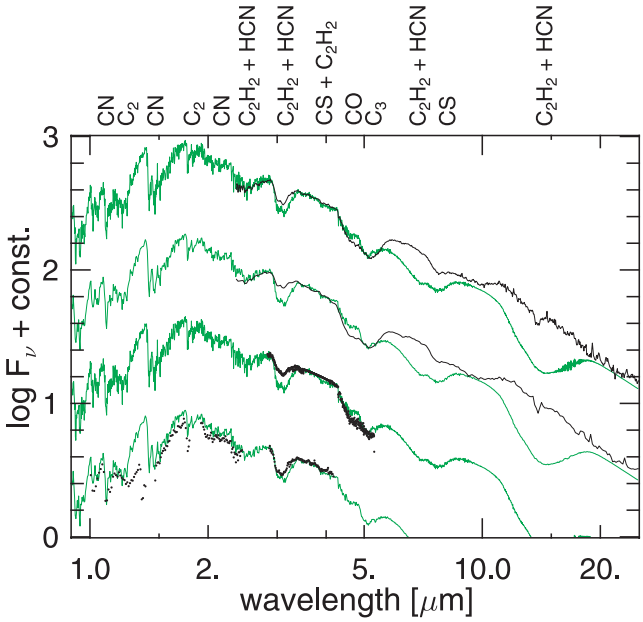

Fig. 9. Comparison of l52t31c14u4pim15 model spectra with observations of V460 Cyg. The model phase is 0.55 in all cases. On top of the figure the *main* contributing molecules are labelled.

4.4.1. Influence of model parameters on the fit

For V460 Cyg we obtained a best simultaneous fit of all observed spectra and colour measurements with model l52t34c12u2p ($T_\star = 3400$ K, $L_\star = 5200\,L_\odot$, $M_\star = 1\,M_\odot$, C/O = 1.2 for the hydrostatic initial model; $P = 148$ d, $\Delta u_\mathrm{p} = 2$ km s^{-1}). The fit is not of very high quality, thus we tried to systematically vary the model parameters within certain ranges. A model with a lower temperature on the one hand improves the quality of the fit of the overall shape of the spectral energy distribution at wavelengths shortwards of 2.5 μm, but on the other hand makes it impossible to fit the observed weak 3 μm C_2H_2/HCN features and it decreases the quality of the fit of the 7 μm region drastically. A model with a higher C/O ratio (1.4 instead of 1.2) improves the fit of the C_3 feature at 5.1 μm and of the C_2 features between 1 and 2 μm, but decreases the quality of the fit in the 7 μm region. Unfortunately we were not able to converge any hydrostatic initial model with $T_\star > 3100$ K and C/O = 1.4 when varying $L_\star$ and $M_\star$ within the range of our grid. The same problem occurs in the calculation of spherical MARCS atmospheres in these parameter ranges (Gautschy-Loidl 2001; Eriksson, private comm.). Thus we calculated a model with C/O = 1.4, lower temperature and higher mass. Figure 9 shows the resulting comparison of synthetic spectra of model l52t31c14u4pim15 ($T_\star = 3100$ K, $L_\star = 5200\,L_\odot$, $M_\star = 1.5\,M_\odot$ and C/O = 1.4 for the hydrostatic initial model; $P = 180$ d, $\Delta u_\mathrm{p} = 4$ km s^{-1}) with the observations of V460 Cyg. We see that although the fit of the overall energy distribution and of the C_3 feature at 5.1 μm is quite good, we are unable to explain the weak observed 3 μm C_2H_2/HCN feature intensities and the absence of the C_2H_2 contribution around 7 μm. While the latter may be well due to the influence of the dust which we can not account for with our dustless l52t31c14u4pm15 model, we can not expect that the contribution of the dust weakens the 3 μm feature intensities to such a degree.

4.5. T Lyr

T Lyr is an irregular variable (Lb) star. Observational data of Baumert (1972), of Lázaro et al. (1994), of Joyce (1998), and one ISO SWS06 spectrum were available. Schöier & Olofsson (2001) list a mass loss rate of $7.0 \times 10^{-8}\,M_\odot$ yr^{-1}. Although we computed various models with different sets of parameters we were not able to find one which represents a fit of high quality covering a large wavelength region, but instead we have several models describing the observations of T Lyr with about equal quality. Thus it is difficult to speak of a "best fit model" in this case. A reasonable fit was obtained with model l52t30c20u2pm20 ($T_\star = 3000$ K, $L_\star = 5200\,L_\odot$, $M_\star = 2\,M_\odot$, C/O = 2.0 for the hydrostatic initial model; $P = 148$ d, $\Delta u_\mathrm{p} = 2$ km s^{-1}). These temperature and C/O ratio values differ significantly from parameter determinations of other authors (see Table 3).

Baumert (1972) measured T Lyr five times between November 1969 and November 1970. We took the maximum and minimum colour values of his measurements, the maximum values are denoted by triangles in Fig. 10, the minimum values by diamonds. Minimum observations and models were forced to have equal flux at 1.0804 μm. We see that the overall shape of the energy distribution is very well represented by our model. The contributions of C_2 at 1.0395 and 1.0544 μm, however, are too strong.

In Fig. 11, one ISO SWS06 spectrum from November 1996, one spectrum from Joyce from September 1991, and one spectrum from Lázaro et al. (1994) observed in 1983 are shown. Observed (black lines) and model (grey lines) spectra were forced to have equal flux at 3.4 μm. The model spectra were rebinned to a resolution of 500 (for comparison with the SWS06 observation) or to a resolution of 250 (for comparison with the Joyce and

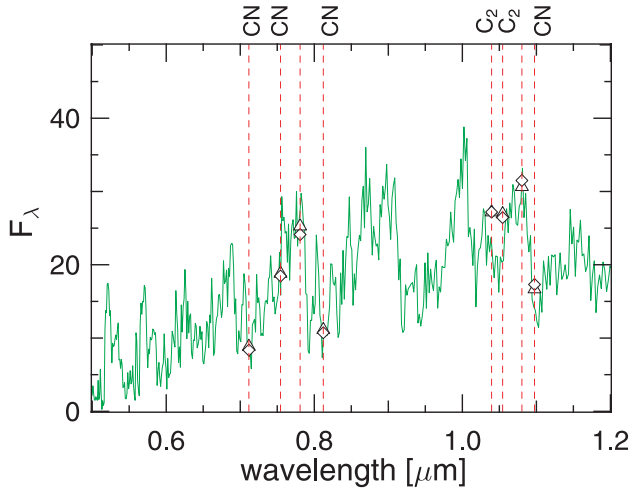

Fig. 10. Comparison of a l52t30c20u2pm20 minimum model spectrum (phase 0.52) with the Baumert observations of T Lyr. The maximum values of his colour measurements are denoted by triangles, the minimum values by diamonds. On top of the figure the *main* contributing molecule is labelled.

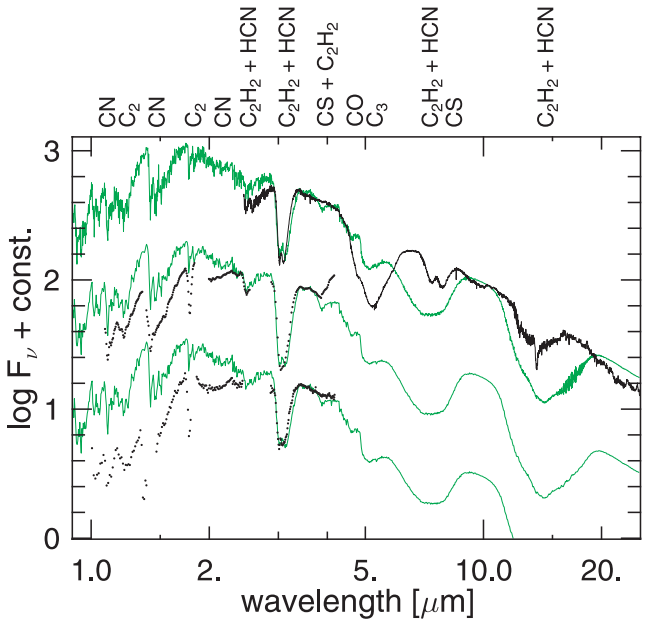

Fig. 11. Comparison of l52t30c20u2pm20 model spectra (grey lines) with the following observational data (black lines) of T Lyr (*from top to bottom*): one ISO SWS06 spectrum, one spectrum from Joyce, and one spectrum from Lázaro et al. (1994). The model phases are (*from top to bottom*): 0.61, 0.52, and 0.09. On top of the figure the *main* contributing molecules are labelled.

Lázaro observations). T Lyr shows strong C_2 bands between 1 and 2 μm, strong C_2H_2/HCN absorption features at 3, around 7 and around 14 μm, a strong C_3 feature at 5.1 μm, and no or only a very weak SiC emission feature around 11 μm. Noticeable is the absence of the 3.8 μm feature. Obviously our fit to the observed spectra is of poor quality. We are able to explain the intensities of the 2.5 and the 3 μm C_2H_2/HCN features with this model. Still, choosing a C/O ratio as high as 2.0, we are far from being able to explain the strong observed C_3

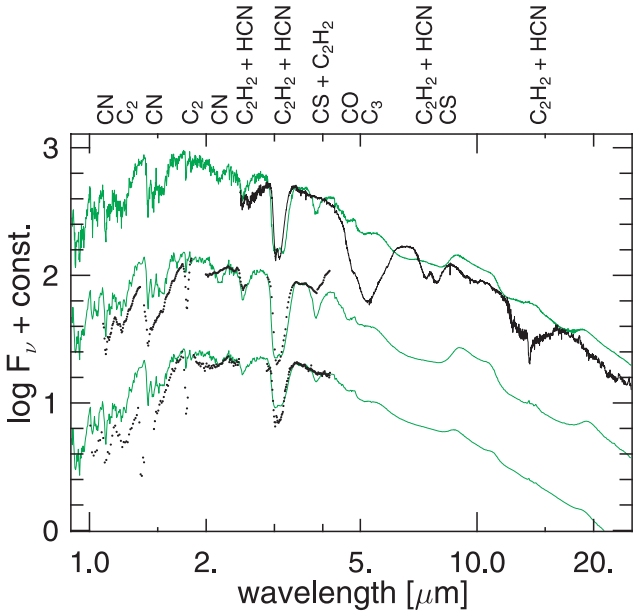

Fig. 12. Comparison of l70t28c16u4 model spectra (grey lines) with observational data (black lines) of T Lyr. The model phases are (*from top to bottom*): 0.09, 0.82, and 0.00. On top of the figure the *main* contributing molecules are labelled.

feature at 5.1 μm while the C_2H_2/HCN absorption predicted by our model in the 7 μm region is too strong and also the overall shape of the energy distribution is poorly represented. The discrepancy at wavelengths longer than 10 μm will be discussed separately in Sect. 6.

4.5.1. Influence of model parameters on the fit

For T Lyr we obtained a reasonable simultaneous fit (according to our criteria) of all observed spectra and colour measurements with model l52t30c20u2pm20 ($T_\star = 3000$ K, $L_\star = 5200\,L_\odot$, $M_\star = 2\,M_\odot$, C/O = 2.0 for the hydrostatic initial model; $P = 148$ d, $\Delta u_p = 2$ km s^{-1}). Due to the low quality of this fit we calculated various models where we varied all model parameters systematically. Choosing a mass of $2\,M_\odot$ instead of 1 enabled us to explain the presence of the strong 3 μm and the simultaneously weak 3.8 μm C_2H_2/HCN feature intensities. A lower $T_\star$ improves the match of the overall energy distribution, but makes it impossible to describe the intensities of the 2.5, 3 and the 3.8 μm C_2H_2/HCN features correctly. One of our models with higher $L_\star$, lower $T_\star$ and $M_\star$ (l70t28c16u4) developed a relatively weak, irregular wind. Figure 12 shows the results of the comparison of the spectra of model l70t28c16u4 ($T_\star = 2800$ K, $L_\star = 7000\,L_\odot$, $M_\star = 1\,M_\odot$ and C/O = 1.6 for the hydrostatic initial model; $P = 390$ d, $\Delta u_p = 4$ km s^{-1}) with the observations of T Lyr.

We see that this model explains the overall energy distribution much better, but longwards of 3.5 μm the quality of the fit is worse than with model l52t30c20u2pm20. The mass loss rate of our l70t28c16u4 model is an order of magnitude higher (6.6×10^{-7}) than the observed one (7×10^{-8}). The low observed mass loss rate of T Lyr tells us that we see basically a pure photospheric 3 and 3.8 μm C_2H_2/HCN feature. This means that $T_\star$

can not be much lower than 3000 K, otherwise one can not explain the observed intensities of these features. On the other hand, the shape of the overall energy distribution suggests a much lower $T_\star$. A possible solution to this puzzle may be that one has to adopt a *much higher* C/O ratio than we did. The strong observed C_2 bands in the wavelength region between 1 and 2 μm as well as the strong C_3 feature at 5.1 μm would at least support the assumption that a C/O ratio of about 3 may be indeed realistic for this star.

5. Comparison between observations and synthetic spectra of models with mass loss

At present, our grid of dynamical models contains mainly dustless and wind-free models which are appropriate to describe relatively hot carbon stars. We focused on these models to perform a detailed comparison with the results of standard hydrostatic spherical models on the one hand, and on the other hand to explain the observed variations of only moderately variable carbon stars more consistently by different phases of one dynamical model instead of a sequence of several hydrostatic models with different effective temperatures.

When we compute models of cool carbon stars which show considerable mass loss in the form of a dust-driven stellar wind, then another set of data enters the calculation which have to be carefully chosen: the micro-physical dust properties. Andersen et al. (2003) have recently shown that the choice of dust material properties is significant for the derived outflow velocities, the degrees of condensation, the resulting mass-loss rates, and hence also for the appearance of our synthetic spectra. Up to now we have used the optical properties of amorphous carbon of Rouleau & Martin (1991) and a value of 2.25 g/cm^3 (which is the value of graphite) for the intrinsic density of the amorphous carbon material for reasons of comparability with our earlier models (this value has been used in many studies because the correct value for amorphous carbon was not known at the time when the first dynamical models were constructed). In a further step we intend to calculate and investigate a grid of dynamical models of cool carbon stars where we use the best available set of micro-physical dust data. Here, we limit the discussion of models with dust-driven winds to qualitative effects on the spectra.

Those of our models which develop a stellar wind extend outwards to temperatures of about 300 K. However, in the calculation of the synthetic spectra, gas opacities are only included down to temperatures of 1000 K. At cooler temperatures dust is likely to dominate the total opacity. The influence of cutting the gas opacities at 1000 K on the synthetic spectra is small: only the 14 μm region is affected in such a way that the resulting emission is slightly weaker[4].

Due to the restrictions mentioned above we will present only two general results in this section which are not critically dependent on the dust data which we are using. In a first step we will compare spectra in the wavelength region between 1 and 25 μm of S Cep with our dynamical model spectra and discuss the influence of the wind on the synthetic spectra. Secondly we show that our cool dynamical models can explain and reproduce a feature at 1.53 μm which is observed in a few cool carbon Miras around minimum light but is not reproduced by hydrostatic model atmospheres.

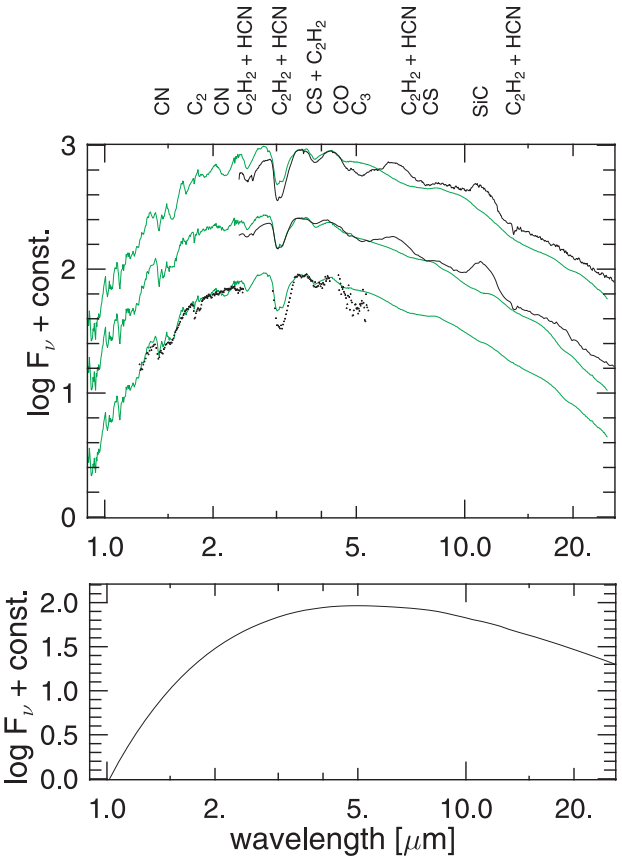

Fig. 13. *Upper panel*: comparison of l10t26c14u4f20pi model spectra (grey lines) with the following observational data (black lines) of S Cep (from top to bottom): one ISO SWS01 spectrum from December 5th 1997 (visual maximum; phase 0.0), one ISO SWS01 spectrum from May 31st 1997 (visual minimum; phase 0.4), and one KAO spectrum from December 13th 1976 (phase 0.56; half way between minimum and maximum – the light curve has a strong bump in the rising branch). The model phases are (from top to bottom): 0.53, 0.89, and 0.70. On top of the figure the *main* contributing molecules are labelled. *Lower panel*: pure dust spectrum of the l10t26c14u4f20pi model at phase 0.53.

5.1. S Cep

Table 2 lists the basic properties of S Cep. We want to stress that we do not intend to present a fit of the observed spectra of S Cep here, but that we want to discuss a few basic properties of the spectra resulting from our dynamical models which show a considerable mass loss rate. Therefore we show a comparison of two ISO SWS01 spectra and one KAO spectrum of S Cep with model l10t26c14u4f20pi in the upper panel of Fig. 13. Observed (black lines) and model (grey lines) spectra were forced to have equal flux at 3.4 μm. The model spectra were rebinned to a resolution of 250 for the comparison with the

[4] Our dustless models are not affected at all because they do not extend outwards to temperatures below 1000 K.

observations. The lower panel of Fig. 13 shows the pure dust spectrum of the l10t26c14u4f20pi model at phase 0.53.

S Cep shows strong C_2H_2/HCN absorption features at 3 and 3.8 μm, and a strong C_3 feature at 5.1 μm. We interpret the spectrum longwards of 5 μm as two strong C_2H_2/HCN absorption bands around 7 and 14 μm, and a strong SiC emission feature around 11 μm. For the determination of the temperature of the star we use as criteria that the 2.5, the 3 and the 3.8 μm C_2H_2/HCN feature should be described properly by our dynamical models as well as the overall shape of the energy distribution. Obviously we fail to match these criteria at least for the phases where S Cep shows a strong 3 μm C_2H_2/HCN feature. When we are able to reproduce the overall energy distribution, the observed spectrum at wavelengths shorter than 2.3 μm and the 3.8 μm C_2H_2/HCN feature correctly (lowest spectrum in Fig. 13), we are unable to reproduce the strong 3 μm C_2H_2/HCN feature as well as the 4.6 μm CO and the 5.1 μm C_3 feature. Another discrepancy, but a more technical one, is, that we can describe the spectrum observed at maximum visual light best with a model from bolometric minimum light and vice versa. While in the observed spectra the 3 and 3.8 μm C_2H_2/HCN features are strongest at visual phase 0.56 (which is half way between the visual maximum and minimum light due to a strong bump in the light curve of S Cep in the rising branch), and weakest at visual minimum light (phase 0.4), our l10t26c14u4f20pi model spectra show the strongest 3 and 3.8 μm C_2H_2/HCN features around bolometric minimum light (phase 0.53) and the weakest ones shortly before the bolometric maximum light (phase 0.89). However, Nowotny et al. (2004), using the same model and comparing the line profile variations of CO and CN with observed ones from S Cep, obtain good quantitative agreement with the observed variations as a function of phase. Only the C_2H_2 features which are formed much further out in the atmosphere and the wind region vary "out of phase" and their variation is very much dependent on the model parameters and sometimes very complex (see also Sect. 4.1 for a discussion of the problem of assigning phases)[5].

When comparing Figs. 4, 6, 8 and 11 (models showing no mass loss) with Fig. 13 (model with mass loss), we see immediately that the mass loss influences the synthetic spectra such that:

- the 3 and 3.8 μm C_2H_2/HCN features become considerably weaker;
- the 4.6 μm CO, the 5.1 μm C_3 and the photospheric C_2H_2 and HCN features around 7 and 14 μm are filled up by emission;
- the maximum of the energy distribution is shifted to longer wavelengths.

The photospheric C_2H_2, C_3 and HCN features become weaker because they are superposed on the continuous dust emission.

[5] E.g. model l52t30c05u4p shows quite irregular variations of the C_2H_2 features, resulting in minimum feature intensities either around phase 0.9 or phase 0.2 and maximum intensities around phase 0.1. On the other hand the feature intensities of these features vary very regularly in model l70t30c11u2 with minimum feature intensities around phase 0.4 and maximum intensities around phase 0.0.

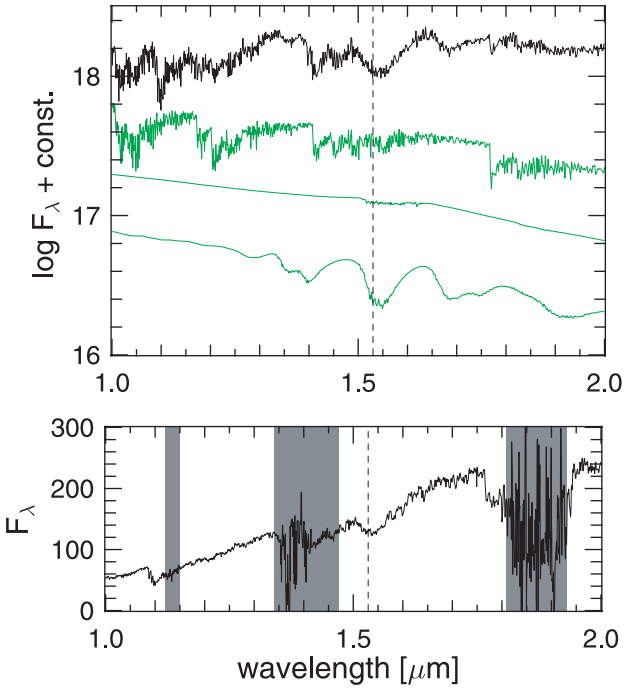

Fig. 14. Full synthetic spectrum at minimum phase of model l70t28c14u5 in the wavelength region between 1 and 2 μm (black line in upper panel) and the contributions of C_2, HCN and C_2H_2 (grey lines; from top to bottom) to the synthetic spectrum. The dotted line marks the short-wavelength edge of the 1.53 μm feature which is observed in cool carbon-rich Miras (e.g. in R Lep; lower panel). The grey shaded areas mark regions of the spectra which are contaminated by the Earth's atmosphere.

The model spectra in Fig. 13 are the first to explain in a self-consistent way how the 3 μm C_2H_2/HCN band can stay strong (as in a pure photospheric spectrum) while the photospheric 7 and 14 μm C_2H_2/HCN bands become almost invisible, and the explanation (as seen by comparison of Figs. 4, 6, 8 and 11 with 13) is routed in the mass loss process. When mass loss sets in, our dynamical frequency-dependent models and corresponding synthetic spectra predict an emission component in the same transitions which cause the photospheric absorption, as a natural consequence of the wind properties. In low resolution the 7 and 14 μm C_2H_2/HCN absorption bands are hence selectively filled in by emission and disappear. We predict that in high resolution one would be able to trace the individual absorption and emission lines side-by-side. However, we also see that our models are not yet able to quantitatively predict quite right the ratio between absorption and emission, since we see that the computed bands become too weak, at least in the case of S Cep with the adopted model.

5.2. The 1.53 μm feature in cool carbon stars

The appearance of a strong band is very remarkable in the dynamical spectra at 1.53 μm of our cool models which show a wind (e.g. l70t28c14u5) at phases close to minimum light.

Figure 14 shows a zoom-in on the appropriate region. Here a minimum (black) spectrum of model l70t28c14u5 and the contributions of the molecules C_2, HCN and C_2H_2 (grey; from

top to bottom) are plotted in the upper panel in the wavelength region between 1 and 2 μm. The dotted line marks the short-wavelength edge of the 1.53 μm feature. Such a feature has been observed in spectra of a few cool carbon-rich Miras (lower panel of Fig. 14), e.g. in R Lep (Lançon & Wood 2000). The feature was tentatively attributed to C_2H by Lançon & Wood (2000) in accordance with the C_2H absorption cross sections presented in Goebel et al. (1983). Goebel et al. (1981), and later Joyce (1998), discussed the possibility of the 1.53 μm feature to be due to a HCN and/or C_2H_2 combination band. This later identification is in agreement with the results of our dynamical computations which attribute the 1.53 μm band to the (020−000) transition of HCN and mainly to the (10100−00000) transition of C_2H_2. These transitions are weak and only at very low temperatures they give rise to enough absorption in order that we can recognise the C_2H_2/HCN feature on top of the C_2 feature at the same position. However, C_2H might potentially also contribute to the 1.53 μm feature since it has a very high partial pressure in our models, but due to the lack of appropriate laboratory data and theoretical computations (see discussion in Loidl et al. 2001), it is not possible to include C_2H in the synthetic spectra at present.

6. The 14 μm feature of carbon stars

In Sects. 4.2 to 4.5, we excluded the discussion of the wavelength region beyond 10 μm. Plane parallel hydrostatic models, spherical hydrostatic models as well as dynamical models without mass loss predict a deep and broad absorption feature due to C_2H_2 and HCN around 14 μm. Compared to the computed spectra, the observed 14 μm band is weak and narrow in most stars, consisting typically of only a small, narrow absorption at 13.7 μm (see e.g. Fig. 8). If the 14 μm band indeed forms at photospheric depths and temperatures as it happens in all self-consistent models without mass loss, then it has to show up as a very broad feature, because many hot-band transitions contribute to the observed band. The anharmonicity constants determining the widths of such an absorption feature in a hot gas are very well determined by laboratory experiments. Therefore, from the discrepancy between observations and models we can conclude that we do not see a pure photospheric spectrum in the long-wavelength region of the ISO spectra.

The idea of a so-called "warm molecular envelope" was introduced in the literature and discussed by several authors (e.g., Tsuji et al. 1997a; Yamamura et al. 1999) in order to explain the discrepancies between computed molecular bands and the observed cool-star spectra. Basically, in the case of a "warm molecular envelope" one or more detached, relatively dense layers of molecular gas above the photosphere are introduced. Temperatures and densities are free parameters which can be adjusted to increase (i.e. absorption) or decrease (i.e. emission) the computed photospheric band intensities until they fit the observed intensities. The disadvantages of such a simplified approach are two: (1) there is no self-consistent physics behind the warm envelope model as it has been presented in the literature, and hence fitting the observed spectrum with such a model cannot reveal physical information about the star, and (2) the intrinsic transition probabilities that give rise to the 3 and 14 μm bands are very similar, and the separation in the excitation energies of the vibrational levels that give rise to the hot-bands are almost identical in the two cases. This means that any temperature inversion in (or dense molecular layer above) the photosphere that weakens the 14 μm band would also weaken the 3 μm band, which is not observed.

Jørgensen et al. (2000) tried to simulate combined dust and gas spectra, firstly by adding a Planck function emission of low temperature to the photospheric spectrum and secondly by using the photospheric dust-free spectra as input to a program that computes dust envelopes. Based on these investigations, they proposed that if the lacking 14 μm photospheric band should be explained by the existence of a separate layer of dust and gas above the photosphere, this layer would have to be around 500 K (to emit radiation obscuring the 14 μm region and giving the right spectral continuum slope) and obscure only about 10% of the surface area (in order to not affect the 3 μm band too much). The weak and sharp 13.7 μm absorption feature would then have to form in cooler layers above the 500 K layer. Indeed, Heske et al. (1989), who mapped the circumstellar CO line emission around TX Psc, interpreted the observed asymmetries as being produced either by a bipolar outflow or by a highly clumped wind. However, these considerations were also based on non-self-consistent physics, and the need for a fully dynamical self-consistent model and spectrum computation in spherical geometry was emphasized.

The results of our dynamical models with mass loss show that the contribution of the dust as well as emission due to the molecules C_2H_2 and HCN fill up the photospheric absorption feature with emission and the only part of the original feature which remains visible is the narrow feature around 13.7 (due to C_2H_2) and 14.0 μm (due to HCN). The l70t28c16u4 model is an interesting transition model. In Fig. 12 we see that in the synthetic spectrum at the top the wings of the 14 μm feature are still in absorption while the "central part" between 13.5 and 14 μm shows already pronounced emission. In the spectrum in the middle the emission contribution is small, but still visible, and in the lowest spectrum the whole feature is filled up with emission and there is basically no feature left.

To investigate the 14 μm feature of carbon stars in more detail, we extracted all stars from the ISO archive for which the 3 and 14 μm region was observed with the SWS06, i.e. with a resolution high enough to distinguish between emission above the surrounding flux which is the sum of molecular absorption filled in with emission and the emission from dust clouds shielding the deep layers. In Fig. 15 all these spectra are plotted with a resolution of 1000, in total there are only six stars where both wavelength ranges are covered. Aoki et al. (1999) discussed already the 14 μm region of TX Psc, V CrB, and SS Vir. They identified HCN emission lines in TX Psc and V CrB. A closer inspection of Fig. 15 suggests that other lines than the ones identified by Aoki and coworkers are in emission as well in the case of S Cep, WZ Cas, TX Psc, and TT Cyg. Therefore, we see that emission is present in the 14 μm region of carbon stars as predicted by our dynamical models, but the observed emission is weak.

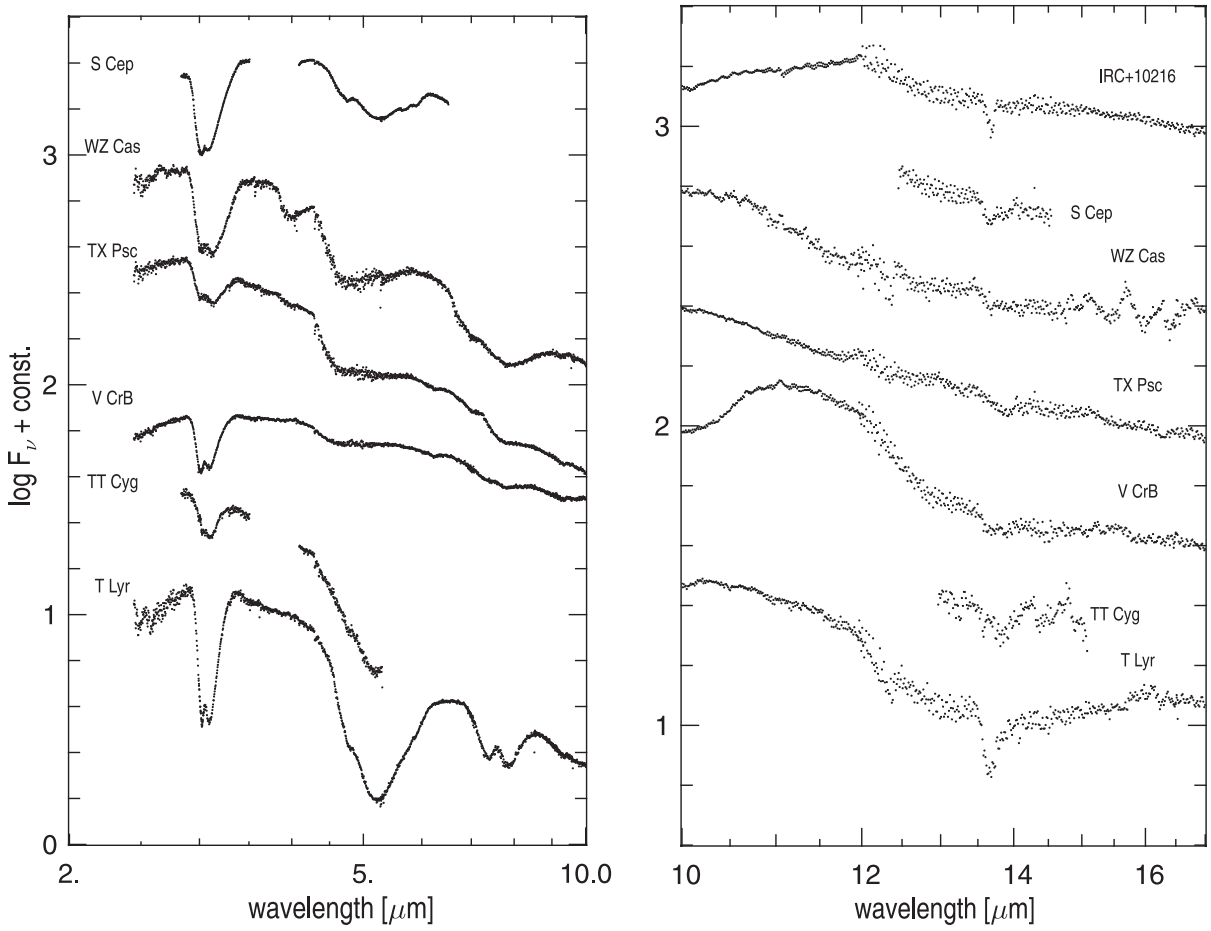

Fig. 15. SWS06 spectra of carbon stars for which the 3 and the 14 μm region was observed simultaneously. The spectra have a resolution of 1000.

T Lyr is the only star in our sample showing a deep 14 μm feature. Additionally, it has strong 3, and 5.1 μm features as well as strong absorption in the 7 to 8 μm region. All of these features, except the 5.1 μm one, are due to a combination of C_2H_2 and HCN. The C_2H_2 contributions are stronger than the HCN ones in T Lyr. Contrary to all other stars in Fig. 15, with the exception of WZ Cas, it shows an additional feature around 12.3 μm. The shape of the spectrum of T Lyr as a whole suggests that we see a relatively pure photospheric spectrum of a cool carbon star. IRC+10216 on the contrary is a very dust enshrouded carbon star. It has basically no features shortwards of 10 μm (therefore it is excluded in the left panel of Fig. 15), but it shows the sharpest C_2H_2 feature at 13.7 μm of all stars in our sample. S Cep and V CrB are cool enough for the contribution of C_2H_2 to dominate the 3 μm feature, both stars show broader absorption around 14 μm than the stars previously discussed. For TX Psc, WZ Cas, and TT Cyg the contribution of HCN dominates the 3 μm feature, but for different reasons: TX Psc is too hot and the C/O ratio is too low in order that considerable amounts of C_2H_2 are formed; TT Cyg is a star with a high C/O ratio, but it is too hot to form huge amounts of C_2H_2; WZ Cas on the other hand is in principle cool enough, but there is not much carbon available to form C_2H_2. TT Cyg is the only star for which the contribution of HCN to the 14 μm feature is stronger than the one of C_2H_2. The 14 μm features of WZ Cas and TX Psc are barely visible.

From our comparison with ISO observations we see that our models without mass loss predict too strong C_2H_2 contributions to the 14 μm region (as well as to the 7 μm region). Our wind models on the other hand predict much too strong emission originating from the outer layers which fills up the photospheric features at wavelengths longwards of 4.5 μm. The pressure-temperature structure of the models where the features form which we see in the spectra longwards of about 4.5 μm is critically dependent on the opacity data of C_2H_2, C_3 and HCN on one hand, and on the other hand on the treatment of the pulsation. We use a piston for the description of the pulsation, which is only a crude approximation. These restrictions make it currently impossible for us to explain observed spectra of carbon stars which show a moderate mass loss rate in detail at wavelengths longwards of 4.5 μm.

7. Conclusions

We present synthetic spectra based on dynamic model atmospheres which couple time-dependent dynamics and frequency-dependent radiative transfer. This is the first time a systematic comparison has been performed between observed spectra and synthetic spectra based on such model

Table 4. Results of our fits.

Star name	$P_{\rm obs}$	$\dot{M}_{\rm obs}$	$T_\star$	$L_\star$	$M_\star$	C/O	$P_{\rm mod}$	$\Delta u_{\rm p}$	$\dot{M}_{\rm mod}$
	[days]	[$M_\odot$ yr^{-1}]	[K]	[$L_\odot$]	[$M_\odot$]		[days]	[km s^{-1}]	[$M_\odot$ yr^{-1}]
TX Psc	–	9.1×10^{-8}	3200	5200	1.0	1.1	295	4	–
WZ Cas	186	6.5×10^{-9}	3000	5200	1.0	1.05	186	6	–
V460 Cyg	180	1.8×10^{-7}	3400	5200	1.0	1.2	148	2	–
	180	1.8×10^{-7}	3100	5200	1.5	1.4	180	4	–
T Lyr	–	7.0×10^{-8}	3000	5200	2.0	2.0	148	2	–
	–	7.0×10^{-8}	2800	7000	1.0	1.6	390	4	6.6×10^{-7}

atmospheres. Also the spectrum computation itself is improved compared to our earlier works, by being spherical (instead of plane parallel) and by including dust opacities for amorphous carbon. Spectra of the hydrostatic initial models which can be directly compared to those of well-tested MARCS models yield results comparable to those of the MARCS models.

We compare our results with various kinds of observational data in the wavelength region between 0.5 and 25 μm at several phases of TX Psc, WZ Cas, V460 Cyg, T Lyr and S Cep. Table 4 summarizes basic properties of our sample stars and the temperatures, luminosities, C/O ratios and periods of our best fitting models.

For the first time we are able to present simultaneous self-consistent fits of high quality to various kinds of observational data in the wavelength region between 0.5 and 5 μm for TX Psc and between 0.5 and 10 μm for WZ Cas, resulting from *one time-dependent dynamical model* for each of the two stars. Previously in the literature, each spectrum has been fitted individually, using hydrostatic models with different stellar parameters. This leads not only to different values of the estimated fundamental stellar parameters for each spectrum of a given star, but frequently also to different best fit abundances, quantities which can clearly not be dependent on phase.

In the wavelength region shortward of $\approx$10 μm we are able to fit the observed colours and spectra well; in particular for the stars with the highest temperatures and/or lowest C/O ratios. Longward of 10 μm the spectra based on our dust-free windless dynamical models are dominated by a clear photospheric absorption spectrum with a broad and intense C_2H_2/HCN band around 14 μm, in pronounced contrast to the observed spectra which (at the relatively low resolution of ISO) are more continuum-like with a weak and narrow C_2H_2 feature at 13.7 μm. This discrepancy between observed and computed infrared spectra of carbon stars is well known from hydrostatic models too.

From observations it is estimated that all the stars we have modelled in this paper have a wind. However the observed mass loss rate of S Cep is between one and almost 3 orders of magnitude higher than those of the other stars. For the coolest star in our analysis, S Cep, which has also a high C/O ratio, we can describe the available spectra of the region shortward of $\approx$4 μm with different phases of a model with $T_* = 2600$ K. The effect of dust formation is crucial for understanding the discrepancy in the 14 μm region. As a consequence of the formation of a dust driven wind, our synthetic spectra of S Cep show emission longward of $\approx$4 μm. This emission fills up the strong photospheric absorption bands of C_2H_2/HCN at 7 and 14 μm. Although the presented model is not in perfect quantitative agreement with the observed spectra, it offers the first self-consistent qualitative model explanation of why we see a clear photospheric spectrum at 3 μm (and at shorter wavelengths) but strong non-photospheric contributions of the same molecules at 14 μm in ISO's carbon star spectra. The success of the S Cep model regarding a self-consistent explanation of the full spectrum of this star leads us to expect that future modelling of weak winds in other stars may solve the longstanding problem of the seeming inconsistency between the ISO spectral features short-ward and long-ward of $\approx$5 μm in all observed carbon stars.

Finally, we notice that some of our cool dynamical models with winds reproduce a feature at 1.53 μm, which has been observed in several cool carbon stars but not yet been identified with certainty. In our model this band arises from a combination of overlapping transitions of C_2H_2 and HCN.

Acknowledgements. This work was partly supported through FWF-project P14365-PHY. We thank Kjell Eriksson for helpful discussions about hydrostatic model atmospheres and Thomas Lebzelter and Walter Nowotny for fruitful comments.

References

Andersen, A. C., Höfner, S., & Gautschy-Loidl, R. 2003, A&A, 400, 981
Aoki, W., Tsuji, T., & Ohnaka, K. 1998, A&A, 340, 222
Aoki, W., Tsuji, T., & Ohnaka, K. 1999, A&A, 350, 945
Baumert, J. H. 1972, Ph.D. Thesis, Ohio State University
Beach, T. E., Willson, L. A., & Bowen, G. H. 1988, ApJ, 329, 241
Bessell, M. S., Brett, J. M., Scholz, M., & Wood, P. R. 1989, A&A, 213, 209
Bessell, M. S., Scholz, M., & Wood, P. R. 1996, A&A, 307, 481
Bowen, G. H. 1988, ApJ, 329, 299
Bowen, G. H., & Willson, L. A. 1991, ApJ, 375, L53
Chandra, S., Kegel, W. H., Le Roy, R. J., & Hertenstein, T. 1995, A&AS, 114, 175
Costes, M., Naulin, C., & Dorthe, G. 1990, A&A, 232, 270
de Graauw, T., Haser, L. N., Beintema, D. A., et al. 1996, A&A, 315, L49
Fleischer, A. J., Gauger, A., & Sedlmayr, E. 1992, A&A, 266, 321
Gail, H. P., & Sedlmayr, E. 1988, A&A, 206, 153

Gauger, A., Gail, H. P., & Sedlmayr, E. 1990, A&A, 235, 345
Gautschy-Loidl, R. 2001, Ph.D. Thesis, University of Vienna
Goebel, J. H., Bregman, J. D., Cooper, D. M., et al. 1983, ApJ, 270, 190
Goebel, J. H., Bregman, J. D., Goorvitch, D., et al. 1980, ApJ, 235, 104
Goebel, J. H., Bregman, J. D., Strecker, D. W., Witteborn, F. C., & Erickson, E. F. 1978, ApJ, 222, L129
Goebel, J. H., Bregman, J. D., Witteborn, F. C., & Taylor, B. J. 1981, ApJ, 246, 455
Goorvitch, D., & Chackerian, C. Jr. 1994, ApJS, 91, 483
Gustafsson, B., Bell, R. A., Eriksson, K., & Nordlund, Å. 1975, A&A, 42, 407
Gustafsson, B., & Höfner, S. 2004, in Asymptotic Giant Branch Stars, ed. H. J. Habing, & H. Olofsson (Springer), 149
Heske, A., Te Lintel Hekkert, P., & Maloney, P. R. 1989, A&A, 218, L5
Hofmann, K.-H., Scholz, M., & Wood, P. R. 1998, A&A, 339, 846
Höfner, S. 1999, A&A, 346, L9
Höfner, S., & Dorfi, E. A. 1997, A&A, 319, 648
Höfner, S., Gautschy-Loidl, R., Aringer, B., & Jørgensen, U. G. 2003, A&A, 399, 589
Höfner, S., Jørgensen, U. G., Loidl, R., & Aringer, B. 1998, A&A, 340, 497
Hron, J., Loidl, R., Höfner, S., et al. 1998, A&A, 335, L69
Iben, I. 1984, ApJ, 277, 333
Irwin, A. W. 1981, ApJS, 45, 621
Irwin, A. W. 1988, A&AS, 74, 145
Jørgensen, U. G. 1989, ApJ, 344, 901
Jørgensen, U. G. 1997, in Molecules in Astrophysics: Probes and Processes, ed. E. F. van Dishoek (Kluwer), Proc. IAU Symp., 178, 441
Jørgensen, U. G., & Larsson, M. 1990, A&A, 238, 424
Jørgensen, U. G., Hron, J., & Loidl, R. 2000, A&A, 356, 253
Jørgensen, U. G., Johnson, H. R., & Nordlund, Å. 1992, A&A, 261, 263
Jørgensen, U. G., Larsson, M., Iwamae, A., & Yu, B. 1996, A&A, 315, 204
Joyce, R. R. 1998, AJ, 115, 2059
Lambert, D. L., Gustafsson, B., Eriksson, K., & Hinkle, K. H. 1986, ApJS, 62, 373
Lançon, A., & Wood, P. 2000, A&AS, 146, 217
Lázaro, C., Hammersley, P. L., Clegg, R. E. S., et al. 1994, MNRAS, 269, 365
Loidl, R., Höfner, S., Jørgensen, U. G., & Aringer, B. 1999, A&A, 342, 531
Loidl, R., Lançon, A., & Jørgensen, U. G. 2001, A&A, 371, 1065
Nowotny, W., Aringer, B., Höfner, S., et al. 2004, A&A, in preparation
Ohnaka, K. 1997, Ph.D. Thesis, University of Tokyo
Ohnaka, K., Tsuji, T., & Aoki, W. 2000, A&A, 353, 528
Olofsson, H., Eriksson, K., Gustafsson, B., & Carlström, U. 1993, ApJS, 87, 267
Querci, F., Querci, M., & Tsuji, T. 1974, A&A, 31, 265
Rouleau, F., & Martin, P. G. 1991, ApJ, 377, 526
Sauval, A. J., & Tatum, J. B. 1984, ApJS, 56, 193
Schöier, F. L., & Olofsson, H. 2001, A&A, 368, 969
Strecker, D. W., Erickson, E. F., & Witteborn, F. C. 1978, AJ, 83, 26
Tej, A., Lançon, A., & Scholz, M. 2003, A&A, 401, 347
Tsuji, T. 1973, A&A, 23, 411
Tsuji, T., Ohnaka, K., & Aoki, W. 1997a, Proc. of Diffuse Infrared Radiation and the IRTS, ed. H. Okuda, T. Matsumotoand, & T. Roellig, ASP Conf. Ser., 124
Tsuji, T., Ohnaka, K., Aoki, W., & Yamamura, I. 1997b, A&A, 320, L1
Windsteig, W., Dorfi, E. A., Höfner, S., Hron, J., & Kerschbaum, F. 1997, A&A, 324, 617
Wing, R. F. 1971, Proc. of the Conference on Late-Type Stars, ed. G. W. Lockwood, & H. M. Dyck, Kitt Peak Nat. Obs. Contr., 554, 145
Winters, J. M., Fleischer, A. J., Le Bertre, T., & Sedlmayr, E. 1997, A&A, 326, 305
Winters, J. M., Le Bertre, T., Jeong, K. S., Helling, C., & Sedlmayr, E. 2000, A&A, 361, 641
Yamamura, I., de Jong, T., Onaka, T., Cami, J., & Waters, L. B. F. M. 1999, A&A, 341, L9